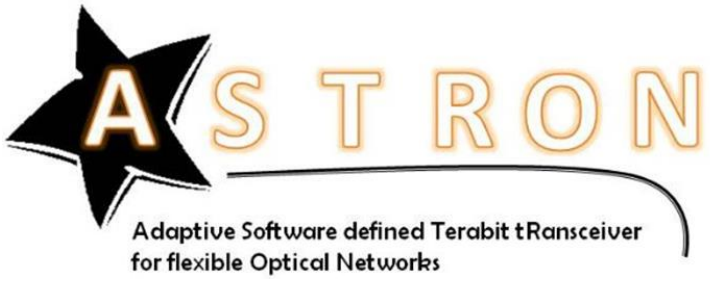

ADAPTIVE SOFTWARE DEFINED TERABIT TRANSCEIVER FOR FLEXIBLE OPTICAL NETWORKS

FP7-ICT-GA 318714

SPECIFIC TARGETED RESEARCH PROJECT (STREP)INFORMATION & COMMUNICATION TECHNOLOGIES (ICT)

Performance evaluation of software defined transmitter and receiver

D6.6

Document Type:	Deliverable
Dissemination Level:	RE[1]
Lead Beneficiary:	UCL
Contact Person:	Robert Killey (email: r.killey@ucl.ac.uk)
Delivery Due Date:	1/04/2016
Submission date:	1/04/2016
Contributing institutes:	TECHNION, UCL, RM3, AIT, FINISAR
Authors:	Moshe Nazarathy (TECHNION), Alex Tolmachev (TECHNION), Robert Killey (UCL), M. Sezer Erkilinç (UCL), Julian Hoxha (RM3), Gabriella Cincotti (RM3), Vassiliki Vgenopoulou (AIT), Ioannis Tomkos (AIT), Shalva Ben-Ezra (FINSAR)
Reviewers:	Roberto Magri (TEI)

[1]PU = Public
PP = Restricted to other programme participants (including the Commission Services)
RE = Restricted to a group specified by the consortium (including the Commission Services)
CO = Confidential, only for members of the consortium (including the Commission Services)

Abstract

This report the design and implementation of a terabit-capacity optical testbed for testing the software defined ASTRON devices. The performance of the ASTRON transceiver concept was tested in long haul and long reach access transmission experiments, assessing its robustness to impairments including dispersion and fibre nonlinearity. The experiments on long haul transmission utilised both straight-line and recirculating loop setups, and tested the DSP algorithms using both offline processing and real-time processing using field programmable gate array devices. Additionally, both direct detection and coherent modulation formats have been demonstrated in passive optical networks (PON), as well a hybrid approach using both digital and optical fast Fourier transform. Finally, field-trial experiments have been carried about to demonstrate a novel architecture based on all-optical fractional Fourier transform. At the transmitter, several subcarriers have been transmitted in parallel using an optical orthogonal frequency division multiplexing (OFDM) approach, and are serially received as a Nyquist optical time division multiplexing (OTDM) signal.

The ASTRON Project Consortium

No	Partner Name	Short Name	Country
1	OPTRONICS TECHNOLOGIES A.B.E.T.E.	OPTRONICS	Greece
2	FINISAR ISRAEL LTD	FINISAR	Israel
3	FRAUNHOFER-GESELLSCHAFT ZUR FOERDERUNG DER ANGEWANDTEN FORSCHUNG E.V	HHI	Germany
4	RESEARCH AND EDUCATION LABORATORY IN INFORMATION TECHNOLOGIES	AIT	Greece
5	UNIVERSITY COLLEGE LONDON	UCL	United Kingdom
6	UNIVERSITA DEGLI STUDI ROMA TRE	RM3	Italy
7	ALBIS OPTOELECTRONICS AG	ALBIS	Switzerland
8	AIFOTEC FIBEROPTICS AG	AIFOTEC	Germany
9	ERICSSON TELECOMUNICAZIONI	TEI	Italy
10	NATIONAL INSTITUTE OF INFORMATION AND COMMUNICATIONS TECHNOLOGY	NICT	Japan
11	OPTOSCRIBE LTD	OPTOSCRIBE	United Kingdom
12	TECHNION	TECHNION	Israel

"The research leading to these results has received funding from the European Community's Seventh Framework Programme (FP7/2007-2013) under grant agreement n° 318714".

Revision History

No.	Version	Author(s)	Date
1	0.1	Moshe Nazarathy (TECHNION), Alex Tolmachev (TECHNION), Robert Killey (UCL), M. Sezer Erkilinç (UCL), Julian Hoxha (RM3), Gabriella Cincotti (RM3), Vassiliki Vgenopoulou (AIT), Ioannis Tomkos (AIT), Shalva Ben-Ezra (FINISAR)	
	Comments:	Initial Release	
2	0.2	Moshe Nazarathy (TECHNION), Alex Tolmachev (TECHNION), Robert Killey (UCL), M. Sezer Erkilinç (UCL), Julian Hoxha (RM3), Gabriella Cincotti (RM3), Vassiliki Vgenopoulou (AIT), Ioannis Tomkos (AIT), Shalva Ben-Ezra (FINISAR)	31/03/16
	Comments:	**Final version**	
3			
	Comments:		
4			
	Comments:		

Table of Contents

1. Executive Summary

The performance of the ASTRON software defined transceiver concept was assessed in long haul and long reach access transmission experiments, to determine its robustness to impairments including dispersion and fibre nonlinearity. The experiments on long haul transmission were based on both straight-line and recirculating loop setups, and tested the DSP algorithms using both offline and real-time processing using field programmable gate array devices. In recirculating loop experiments with offline DSP, a single channel polarization division multiplexed optically-shaped orthogonal frequency division multiplexed 16-ary quadrature amplitude modulated (PDM OS-OFDM PDM-16QAM) signal was successfully transmitted over 800 km of standard SMF, and 25 GHz-spaced 4x20 GBd PDM OS-OFDM 16QAM WDM signals were successfully transmitted over 400 km of standard SMF with a Q^2-factor of 13.5 dB. For the real time DSP demonstration, all receiver functions (except for duplicating identical processor modules for all sub-bands) were implemented using just three field programmable gate arrays (FPGAs), achieving complete real-time PDM-16QAM Rx over fastest (180 Gb/s) *filter-bank* hardware reported to date, at a record 1.06 samples/symbol (with a spectral efficiency of 7.3 b/s/Hz). We also showed that the filterband complexity and sampling rate savings imply that an ASIC implementation of the ASTRON concept receiver would save over 50% of the power of a conventional ASIC.

Additionally, we carried out a performance investigation of the inverse Volterra series transfer function nonlinear equalizer (IVSTF-NLE), and digital back-propagation by split-step Fourier algorithm (DBP-SSF) in a 3-channel, 4-band OFDM transmission, to assess the improvements possible through the compensation of fibre nonlinearity.

Focussing on the all-optical OFDM (AO-OFDM) technology developed by Roma3 and NICT, both direct detection and coherent modulation formats have been demonstrated for passive optical networks (PON), as well a hybrid approach using both digital and optical fast Fourier transform. Field-trial experiments have been carried about to demonstrate a novel architecture based on all-optical fractional Fourier transform. At the transmitter, several subcarriers have been transmitted in parallel using an optical orthogonal frequency division multiplexing (OFDM) approach, and are serially received as a Nyquist optical time division multiplexing (OTDM) signal. Experiments were performed on a 16 subcarrier, 12.5 GHz spaced optical OFDM system, using Lithium Niobate phase modulators, with a 12.5 GHz bandwidth. Additionally, we have developed a Nyquist optical time division multiplexing (N-OTDM) technique combined with OFDM and have carried out a field trial of a 4-channel 40 Gb/s OFDM/N-OTDM transmission system, over the 89.2-km JGN X test bed in Japan.

2. Design and implementation of terabit-capacity optical testbeds

A schematic of the wavelength division multiplexed (WDM) 20 GBaud polarization division multiplexed (PDM) OS-OFDM 16QAM optical transmission test-bed is depicted in Fig.1. The output of an external cavity laser (ECL) with a linewidth of 100 kHz was passed through an optical comb generator (OCG). The OCG generates a series of optical carriers at a fixed frequency spacing, generated from a single seed laser. It consisted of two cascaded Mach-Zehnder modulators and a phase modulator, all driven by using an amplified sinusoidal wave generated by a RF generator, phase shifters and a frequency doubler, as shown in Fig. 2. The frequency spacing is determined by the RF generator and wide bandwidth comb was ensured by using multiple cascaded modulators. The phase modulator was

driven by the 2nd harmonic (using a frequency doubler) with a 180° phase shift and an amplitude of 1/16 (12 dB difference) in order to have a better approximation to a quadratic temporal phase, and consequently, to achieve better comb flatness. Since the generated carriers are copies of the seed laser, they are frequency- and phase-locked. An advantage of using OCG in WDM systems is that any fluctuation and/or frequency drift in the seed laser results in the same fluctuation and or frequency drift of the whole comb, potentially avoiding an extra crosstalk between the optical channels. Four frequency locked comb lines with a channel spacing of 25 GHz, a standard ITU-T grid for ultra-dense WDM systems, are generated using the OCG, as described above. A high resolution liquid crystal on silicon (LCOS) optical filter (Finisar WaveShaper 4000S Multiport Optical Processor) was used to achieve a flat comb (limiting the number of comb lines to four) and maintain the power variation across the channels within 1 dB in order to demonstrate the effectiveness of fiber nonlinearities on the performance of WDM OS-OFDM system. Odd ($\lambda_{1,3}$) and even ($\lambda_{2,4}$) lines were separated using three cascaded Kylia micro-interferometer interleavers with a suppression of 40 dB to allow independent modulation with uncorrelated bit sequences (depicted as the demultiplexing stage in Fig.1). Subsequently, the comb lines are used as the source lasers for the IQ-modulators, as shown in Fig.1.

The odd and even lines were independently modulated using two IQ modulators. Initially, the signal waveforms used for driving the IQ-modulators were generated offline using the software tool, Matlab, and subsequently, the waveforms were uploaded to the memory of a pair of Xilinx Virtex-5 field-programmable gate arrays (FPGAs) to drive the digital-to-analogue converters (DACs) (an electrical bandwidth of 15 GHz), operating at 20 GSa/s. The DSP for signal generation is described in detail in deliverable D5.5. The IQ-modulators with a switching voltage (V_π) of 3.5 V were driven by the amplified electrical signals with a peak-to-peak voltage (V_{pp}) of 3.4 V. They were biased close to their quadrature points to achieve approximately linear mapping from the electrical to the optical domain for the OFDM signal and digitally inserted RF-pilot tone. The optical spectrum of the transmitted signal, prior to the transmission using the recirculating loop, can be seen in the inset (a) of Fig.1. Although it is expected to have a flat spectrum for an OFDM signal, the limited bandwidth of the DACs caused a frequency roll-off at higher frequencies (subcarriers) of the OFDM spectrum. The modulated odd and even channels were decorrelated by 85 symbols (17 ns) before being coupled and polarization-multiplexed to obtain a 25 GHz-spaced 4x20 GBd PDM OS-OFDM 16QAM signal with a bandwidth of 20 GHz). The second polarization was generated using a polarization multiplexing delay-line emulation stage, as illustrated in Fig.1.

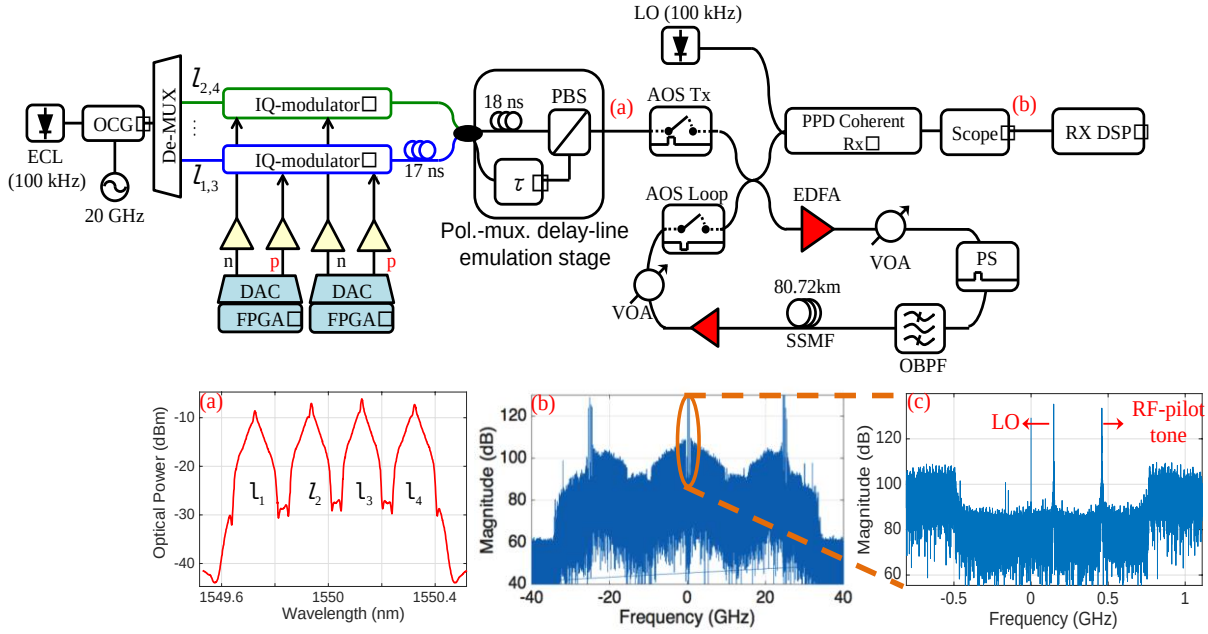

Figure 1: Optical transmission test-bed for WDM OS-OFDM signal. Insets: (a) Transmitted optical spectrum and (b) Received signal and (c) Zoomed into the central channel (channel of interest). ECL: External cavity laser, OCG: Optical comb generator, IQ: In-phase quadrature, FPGA: Field-programmable gate array, DAC: Digital-to-analogue converter, PBS: Polarization beam splitter, AOS: Acoustic-optic switch, EDFA: Erbium-doped fiber amplifier, VOA: Variable optical attenuator, OBPF: Optical band-pass filter, PS: Polarization scrambler, SSMF: Standard single-mode fiber, LO: Local oscillator, PPD: Polarization- and phase-diverse, Rx DSP: Receiver digital signal processing.

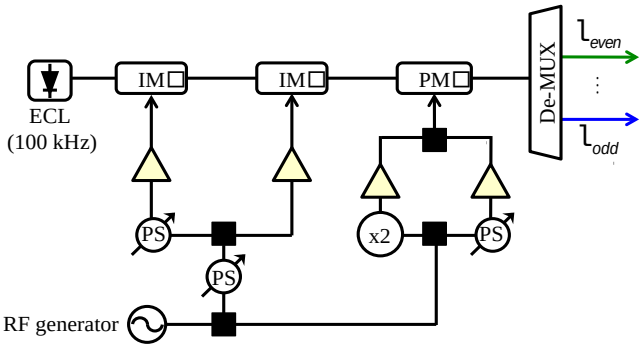

Figure 2: Optical comb generator setup. ECL: External cavity laser, IM: Intensity modulator. PM: Phase modulator. PS: Phase shifter. x2: Frequency doubler. De-MUX: Demultiplexing stage using Kylia interleavers.

The transmission experiment was performed using an optical recirculating loop with a single span of 80.7 km (D_{SSMF} =17 ps/nm/km), as shown in Fig 1. The loop was controlled by two acousto-optic switches (shown as AOS Tx and AOS Loop) to switch from 'signal TX' to 'signal Loop' stage. An optical band-pass filter (OPPF) (Yenista Optics XTM50-Wide) with a 3-dB bandwidth of 200 GHz and a filter edge gradient of 500 dB/nm was used to filter the out-of-band amplified spontaneous emission (ASE)-noise during the transmission. A loop synchronous polarization scrambler (PS) was utilized to randomize the state of polarization of the incoming signal in each span. The launch power into the span was controlled by the variable optical attenuators (VOAs). The fiber loss of 16 dB plus the combined loss of 15 dB from the VOAs, PS, AOSs and OBPF resulted in a total loss per recirculation of 31 dB, which was compensated by two EDFAs with a noise figure of 5 dB, operating at their saturation point (18 dBm output power). A polarization- and phase diverse coherent receiver with intradyne reception (a frequency offset of 200

MHz) was used to detect the transmitted signal. A second laser with a linewidth of 100 kHz was utilized as a local oscillator (LO). Following the coherent detection, the received signal was digitized using an 80 GSa/s real-time sampling oscilloscope with a 33 GHz analogue electrical bandwidth, and subsequently, digital signal processing (DSP) was performed offline using Matlab. The receiver DSP is described in detail in deliverable D5.5.

3. OS-OFDM transmission experiments using offline DSP

The transmission experiments were carried out using the optical recirculating loop, as described in the previous section, and the single channel (band) and WDM system performance were assessed. The single channel PDM OS-OFDM 16QAM signal was successfully transmitted over an 800 km of SSMF. At this distance, a Q^2-factor of 16 dB was achieved and the optimum launch power was found to be 0 dBm, as shown in Fig. 3. Following this, 25 GHz-spaced 4x20 GBd PDM OS-OFDM 16QAM WDM signal was successfully transmitted over a 400 km of SSMF and Q^2-factor 13.5 dB was achieved. The optimum launch power per channel was reduced to -3 dBm due to fiber nonlinearities, mainly the four-wave mixing (FWM) products, as expected. The constellation of the received OS-OFDM DP-16QAM signal at 400 km is shown in the inset of Fig. 3.

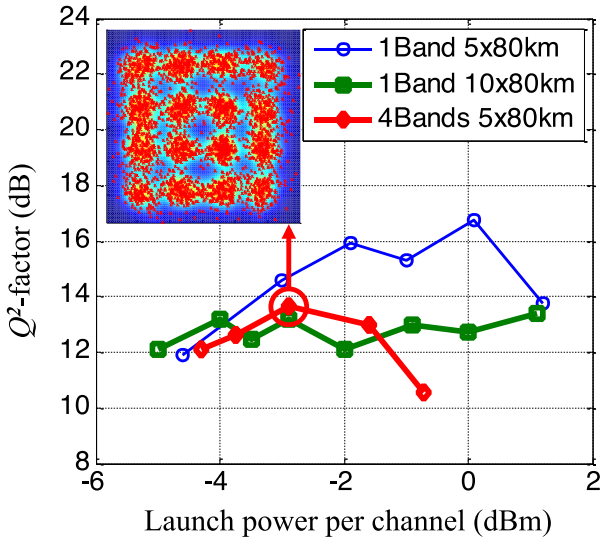

Figure 3: Q^2-factor with respect to launch power per channel. Inset: Received constellation diagram at 400 km (80 km x 5 spans)

The high frequency subcarriers experience a signal-to-noise ratio (SNR) reduction of up to 10 dB compared to the lower frequency subcarriers, as can be observed from the spectra shown in the insets (a) and (b) of Fig.1. This is due to the limited bandwidth of the DACs. To partially overcome this limitation, and consequently, improve the transmission performance, a digital pre-emphasis and/or bit loading can be performed, taking into account the DACs' finite resolution, as explained below.

Ideally, it is desired to have a flat OS-OFDM spectrum after DACs (equal power levels for each subcarrier), similar to the one shown in Fig. 4(a). However, the signal spectrum shown in Fig. 4(b) was obtained due to the DACs' frequency response. The digital pre-emphasis method can be utilized in order to mitigate this frequency roll-off. The frequency response of the DACs used in the transmission experiment can be modeled as a Bessel function. Although it is found that 3rd-order Bessel function offers the optimum performance for Nyquist-shaped single carrier systems, it still needs to be optimized for the OS-OFDM signal by monitoring the system performance.

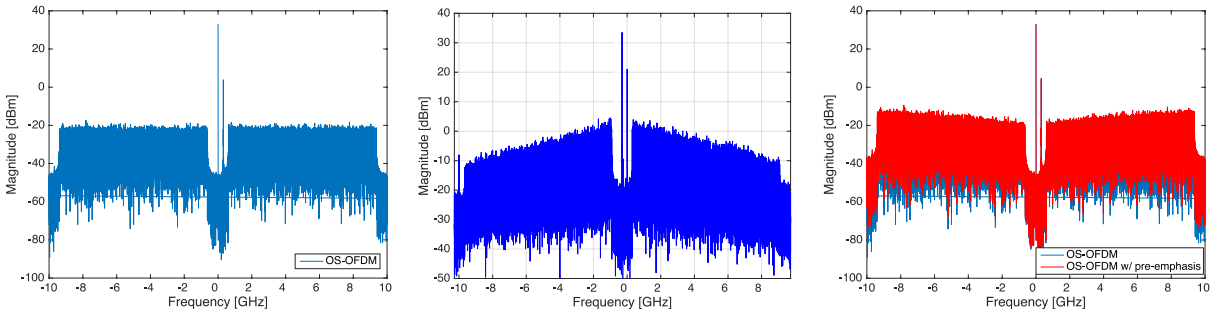

Figure 4: (a) Desired signal and (b) obtained signal after DACs, and (c) signal after digital pre-emphasis is applied.

Furthermore, in addition to digital pre-emphasis, each subcarrier can be modulated with optimally chosen format cardinality, a technique termed bit loading, so that all the subcarriers experience similar bit error probabilities. The format cardinality is chosen depending on the received SNR of each subcarrier, *i.e.*, adaptively modulating the subcarriers based on the DACs' frequency response. The bit-loading is applied using a "water-filling" approach with *M*-QAM modulation where $\log_2(M)$ indicates bits-per-symbol. Conventionally, the Levin–Campello (LC) algorithm is utilized since it provides an optimum discrete bit distribution (finite granularity) assuming the information granularity is the same for all subchannels, which is typically the case. Based on the received SNR of each subcarrier and the SNR threshold values for conventional modulation formats, *e.g.*, BPSK, QPSK, 16-QAM etc., the optimum bit distribution for each subcarrier is decided by the LC algorithm. For instance, to achieve a bit-rate of 160 Gb/s (requiring an average number of bits/symbol per polarization of 4 for a 20 GBd signal), as the subcarriers at higher frequencies experiencing a higher SNR reduction can be allocated with lower numbers of bits/symbol (0, 1, 2 and 3 bits/symbol) per polarization. Conversely, the subcarriers at lower frequencies can be allocated higher bits/symbol (4, 5 and 6 bits/symbol) per polarization. The bit-loading algorithm stops when the maximum achievable total bit rate for a given channel depending on its frequency response is reached.

4. OS-OFDM transmission experiments using real time DSP

Following the experimental assessment of the ASTRON OS-OFDM concept using offline DSP, as described in the last section, the DSP algorithm implementation with real-time processing using field programmable gate array devices was carried out, and the resulting system experimentally tested.

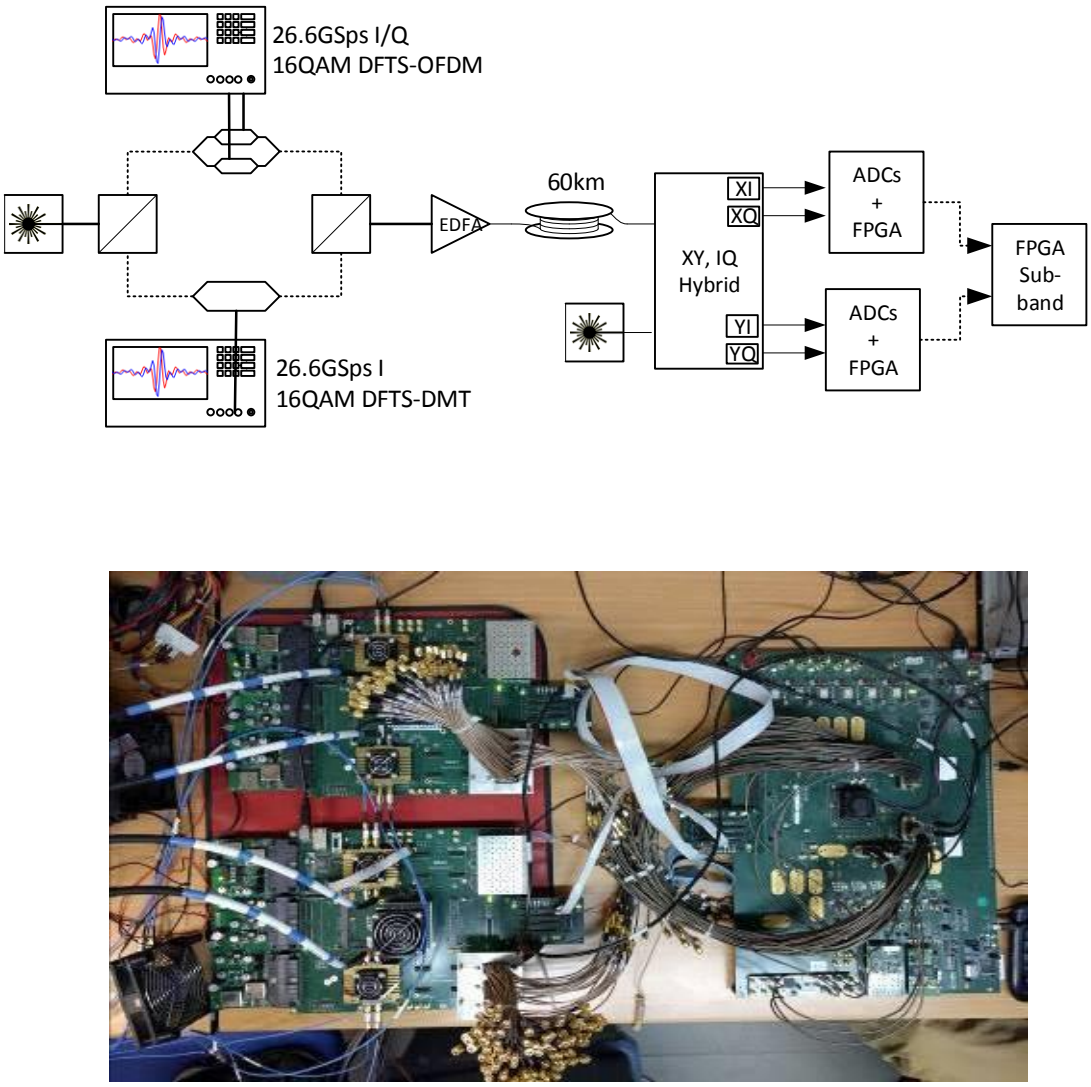

Fig. 5: (left) System block diagram of experimental setup. (right) Real-time 180 Gb/s sub-banded DFT-S OFDM Rx on just 3 Virtex-6 FPGAs

4.1 System Description

The experimental setup (Fig. 5) comprises an optical transmitter (Tx) and Rx for 180 Gb/s data payload over a 60Km SMF optical link. At the Tx side, each transmission band is digitally multiplexed out of 16 *Single Carrier* (SC) sub-bands, realized as DFTS-OFDM 16-QAM per sub-band modulation (Fig. 6 left). Among the 16 sub-bands, 14 of them carry uncorrelated PRBS19 data; two sub-bands (Fig. 6 center) do not carry data but are reserved for special purposes: the 16th wrapped around sub-band provides ADC anti-aliasing filter transition; the 8th sub-band carries two ±415.6 MHz pilots for CFO/phase recovery. The 14 remaining sub-bands carry data, 64-DFTS-OFDM per sub-band, corresponding to 1024 subcarriers for all 16 sub-bands. The *Cyclic Prefix* (CP) is just 8 samples (0.83%). Overall spectral efficiency is 8×14/15×0.9917=7.4b/Hz. Taking into account that just 1% of the transmitted data suffices for channel estimation, our final spectral efficiency is 7.34b/Hz. To reduce the PAPR, we use a low-complexity combination of a *Partial Transmit Sequence* (PTS) algorithm along with optimized clipping (Fig. 6 right). Random phases (±1 factors) are applied to each of the 14 data sub-bands. Out of the 2^{14} possible combinations, we verified that 50 random combinations already provide significant improvement of

several dB, in exchange for moderate extra complexity and 0.5% SE reduction. The last Tx digital stage performs digital high-pass pre-distortion, to compensate for Micram ADC30 and DAC30 roll-off.

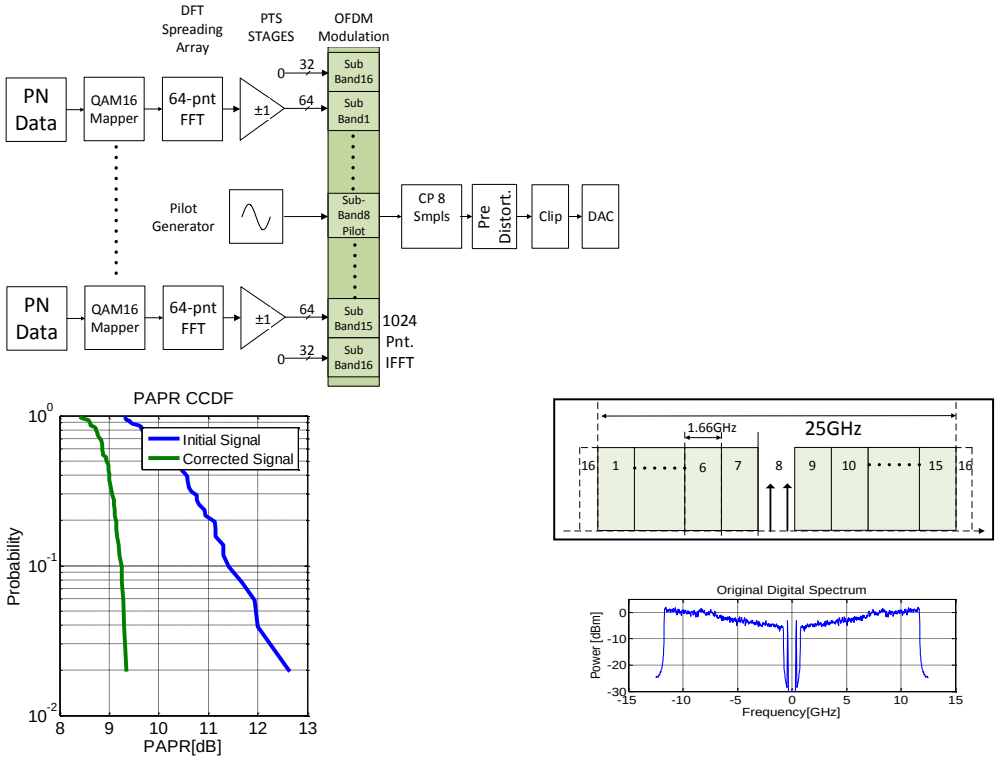

Fig. 6: Transmitter scheme, signal spectrum and results of PTS PAPR reduction for DFT-S OFDM algorithm

The novel Rx DSP is detailed in Fig. 7. The basic functions comprise twice-under-decimated analysis *Filter Banks* (FB) incorporating, at the FB outputs, pilot-assisted carrier frequency offset (CFO) removal and nonlinear phase noise mitigation stages. "Classic" OFDM Rx functions are separately performed on a sub-band basis at 8-fold lower rate. In fact, the two X/Y-FB modules are the only ones operating at full rate. The OFDM receiver functions are: Rx timing sync based on Golay sequence, discrete Fourier transform spread (DFTS)-OFDM de-multiplexing and channel equalization (adaptive least mean squares (LMS) based), QAM16 slicer, BER meter, all efficiently implemented in the FPGA hardware with innovative solutions for the Golay timing. Although we afforded implementing just a single "Sub-band FPGA processor", the other 13 processors would be identical, operating independently and in parallel. The sole sub-band processor is switchable to any filterbank output, enabling to fully evaluate system performance by accessing and demodulating at will any sub-band (1.6 GHz slice) out of the 25 GHz channel spectrum.

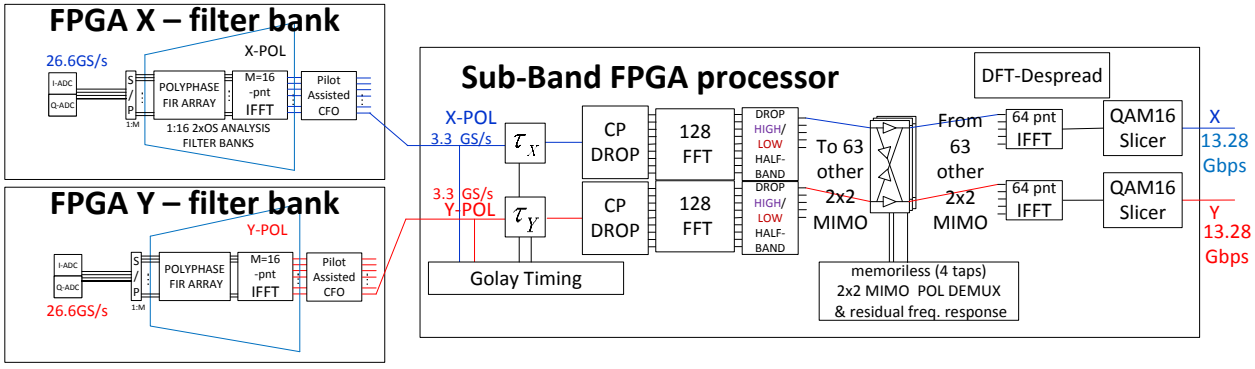

Fig. 7: Sub-banded DFT-S OFDM 180 Gb/s receiver digital signal processing – and its partitioning over 3 FPGAs

4.2 Real-Time Implementation

All receiver functions (Fig. 7) (except for duplicating identical processor modules for all sub-bands) were real-time implemented using *just 3 FPGA chips*. FPGA X/Y interfaces to the ADC chips, performs calibration of internal ADC parameters and carries out IQ gain/phase imbalance correction, at system bring-up. Following IQ-imbalance correction, the data is de-multiplexed into sub-bands. Sub-banding is performed on sets of 16 input samples; due to 2x oversampling, a factor-of-8 rate slow-down is attained. We use 8 time-parallelized filterbank hardware modules (Fig. 8 left), yielding a temporal slow-down factor of 64 at FPGA clock rate of 415.6MHz=(26.6 GS/s)/64. Post filterbank stage, CFO is corrected using data extracted from a pilot sub-band and de-multiplexed (frequency parallelized) over multiple sub-band processor hardware modules - here a single module, the "Sub-Band FPGA" (Fig. 8 right) may be arbitrarily connected to any desired sub-band. This FPGA module also operates at 415.6MHz clock using 8-fold temporal parallelization prior to decimation by factor-of-2 to the sub-band baud rate. Fig. 8 presents the sub-band FPGA chips layout and Table 2 presents FPGA utilization figures of merit (consistent with high hardware efficiency).

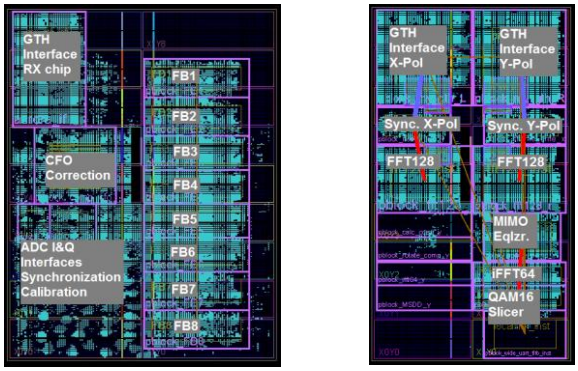

Fig. 8: FPGA layouts: (left) Filter-bank FPGA; (right) Sub-Band FPGA

Table 2: HW Utilization of the Virtex-6 FPGAs

Parameter	Filter Bank FPGA XC6VHX565T	Sub-Band FPGA XC6VHX380T
Logic Blocks-Slices	43139 48%	32789 54%
DSP Multipliers	337 39%	220 25%
Memory (BRAM)	308 20%	160 19%

4.3 Experimental results

To evaluate system performance we measured EVM and BER for each sub-band (Fig. 9 right). A dominant impairment was identified as quantization noise. The estimated ADC ENOB was ~4bits. In actual measurements, the effective ADC noise was higher due to lack of adaptive pre-ADC automatic gain control (AGC) stage. The maximally attainable estimated SNR was ~21dB, whereas the actually back-to-back measured SNR was 18dB, yielding around 3dB implementation penalty. Beyond back-to-back, transmission performance was tested over 60km SMF, yielding minor performance loss, mostly due to setup imperfections. Upon using both polarizations (POL) yielded SNR degradation of ~1dB (likely due to dual-POL PAPR). In all measurements, the tested BER was under the soft FEC 3.8×10^{-3} limit, indicating feasibility for practical optical CO-OFDM implementations at very high spectral and power efficiency.

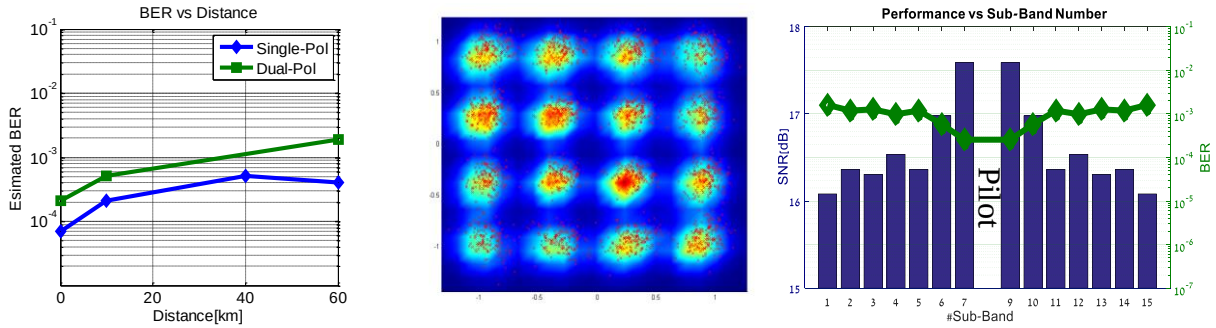

Fig. 9: Experimental results: (left) BER vs reach. (center) Detected constellation after 60km SMF transmission (right) Estimated BER (curve) and SNR per sub-band (bar-chart) over the various sub-bands (degradation away from center due to ADC/DAC roll-off).

4.4 Summary

We demonstrated a complete *real-time* receiver using the fastest (180 Gb/s) *filter-bank* hardware in just 3 FPGAs, at a record 1.06 samples/symbol (7.3 b/s/Hz). The filterbank complexity and sampling rate savings imply that an ASIC implementation of this ASTRON transceiver solution would save over 50% of the power of a conventional ASIC (even with 50% of ASIC occupied by soft FEC).

5. Investigating the full potential of the 3rd-order inverse Volterra series transfer function (IVSTF-NLE) and its variants in the OS-OFDM systems

5.1 Introduction

The motivation for the work described in this section is to answer the key question whether the 3rd-order inverse Volterra series transfer function nonlinear equalizer (IVSTF-NLE) [1] and its variants can be promising candidates for the ASTRON optically shaped (OS)-OFDM systems in terms of performance, computational complexity and power consumption. The performance of the 3rd-order IVSTF-NLE is also compared with the digital backpropagation based on split-step Fourier (DBP-SSF) method [2] with single- and three-steps-per-span in a 3-channel, 4-band OFDM configuration. For brevity, we denote different versions of DBP-SSF equalizers by the abbreviation DBP-SSF_{Nsteps} where N_{steps} is the number of steps per span. The variants of the conventional 3rd-order IVSTF-NLE that are studied are the multistep-per span IVSTF-NLE, the LPF-assisted IVSTF-NLE and the all-band equalization scheme of the former. The results of the following study cases are presented and discussed in the frame of T6.3 of the ASTRON project:

-Performance investigation of the 3rd-order IVSTF-NLE, the DBP-SSF_1 and the DBP-SSF_3 in a 3-channel, 4-band OFDM configuration.
-Performance investigation of the 5-steps-per-span IVSTF-NLE in a 3-channel, 4-band OFDM configuration.
-Performance investigation of the low-pass filter (LPF) assisted IVSTF-NLE by varying the bandwidth, the order of the LPF and the steps-per-span in a 3-channel, 4-band OFDM configuration.
-Performance investigation of the band-by-band and all-band equalization scheme of the IVSTF-NLE in single- and 3-channel, 4-band OFDM configuration
-Evaluation of computational complexity of the IVSTF-NLE, the single- and the 3-steps-per-span DBP-SSF (T2.4).
-Estimation of the power consumption considering a 45 nm ASIC technology (T2.4).

5.2 Results

In this section, we present and discuss the physical limits of the DBP-SSF_1, the DBP-SSF_3, 3rd-order IVSTF-NLE nonlinear equalizers and its variants after (10×100) km of SSMF in two different scenarios:

-Single-channel, 4-band OFDM accommodating 400 Gb/s net rate.
-3-channel, 4-band OFDM accommodating in total 1.2 Tb/s net rate.

In the first scenario, the cross-phase modulation (XPM) and four-wave mixing (FWM) become negligible while in the second scenario, the non-linear effects are exacerbated coming from the channel itself but also from its nearest neighbors. In the coherent receiver, IVSTF-NLE and DBP-SSF_{Nsteps} equalizers are placed at the initial stages of digital signal processing (DSP), where dispersion compensation is usually performed [3].

In order to study the worst case of intra-channel nonlinearities, we have only detected the 3rd sub-band, since inner sub-bands are affected more by inter-channel nonlinear impairments compared to outer sub-bands. To compare the performance of the various equalizers, we use the Q-factor as a figure of merit, which is related to BER through $Q=20\log[\sqrt{2}\mathrm{erfc}^{-1}(2BER)]$ [3], where erfc(x) is the complementary error function [4]. The optimum Q-factor is evaluated by sweeping the nonlinear adjustable parameter *c* [1]. The net Q-factor improvement is obtained by subtracting the maximum Q-factor values in dB at the optimum launch powers with and without nonlinear compensation, respectively. In all cases, the measurements are obtained with the minimum number of samples per symbol (SpS) which is equal to 1.5.

5.2.1 Performance investigation of the IVSTF-NLE, the DBP-SSF_1 and the DBP-SSF_3 in a 3-channel, 4-band OFDM transmission

Fig. 10 shows representative plots of the Q-factor vs. input power per band for a 3-channel, 4-band configuration after equalization. Both the IVSTF-NLE and the DBP-SSF_{Nsteps} methods provide almost identical Q-factor improvement (i.e., ~0.45 dB), whereas the optimum input power is increased by ~0.5 dB. This improvement is rather modest compared to what one might have expected due to the detection and compensation of only one OFDM sub-band which cannot counteract inter-band nonlinearities. It is worth noting that, for WDM transmission, the performance of the IVSTF-NLE is almost identical to that of the DBP-SSF_1. Additionally, the performance of the DBP-SSF method improves slightly with the number of steps per span and saturates at three steps per span. Nevertheless, the DBP-SSF_3 is marginally more powerful than the DBP-SSF_1 at the expense of higher computational complexity.

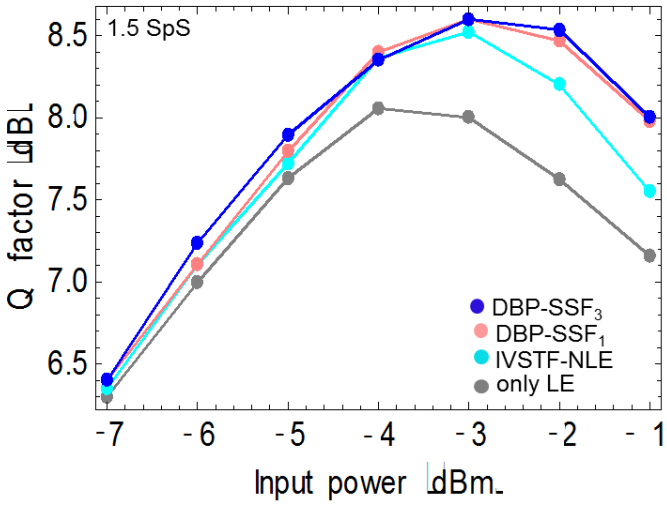

Fig. 20. Q-factor vs. input power per band without/with IVSTF-NLE and DBP-SSF$_{1,3}$ in 3-channel, 4-band configuration after 10×100 km SSMF link.

5.2.2 Performance investigation of the 5-steps-per-link IVSTF-NLE in a 3-channel, 4-band OFDM transmission

In Fig. 11, we show the performance of the 5-steps-per-link IVSTF-NLE (i.e. 2 spans per step) in comparison with the conventional 3rd-order IVSTF-NLE after 10×100 km of SSMF link using the minimum possible number of SpS. The multistep-per-span IVSTF-NLE is providing only 0.33 dB Q-factor improvement, at the optimum input power, which is ~0.2 dB lower compared to the performance of the conventional IVSTF-NLE.

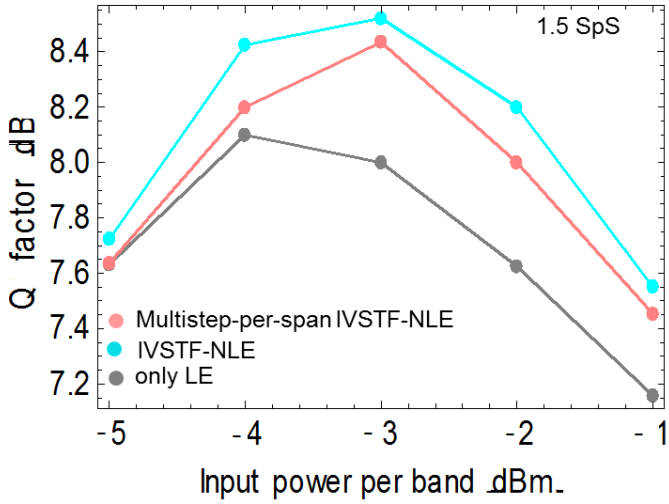

Fig. 11. Q-factor vs. input power per band without/with IVSTF-NLE and multistep-per-span IVSTF-NLE in 3-channel, 4-band configuration after 10×100 km SSMF link.

5.2.3 Performance investigation of the low-pass filter (LPF) assisted IVSTF-NLE by varying the bandwidth, the order of the filter and the steps-per-span in a 3-channel, 4-band OFDM configuration

In this study case, we test the performance of a variant of the 3rd-order IVSTF-NLE by inserting a LPF right before the nonlinear stage of the equalizer so as to reduce the high-frequency components

of the intensity waveform before the calculation of the nonlinear phase correction according to [5]. The LPF that we use for this investigation has the following transfer function:

$$H(f) = exp\left(-\frac{f}{B}\right)^{m}$$

where m is the order of the filter, $B = \sqrt{2}\left(\frac{f_s}{2}\right)$ is the bandwidth of the filter and f_s is the bandwidth of each sub-band.

In Fig. 12, we show the performance of the LPF-assisted IVSTF-NLE using a LPF of 1st -order, 1-step-per-span and increasing bandwidth (i.e. B, 2×B, 3×B and 4×B). We compare their performance with the performance of the conventional IVSTF-NLE after 10×100 km. The performance of the LPF-assisted IVSTF-NLE improves almost negligibly as we increase the bandwidth of the LPF. More specifically, when the bandwidth is B the Q-factor improvement is only ~0.4 dB while for $B \times 5$, it increases up to 0.5 dB

In Fig. 13, the 1st-order LPF-assisted IVSTF-NLE is tested with a larger step size (i.e. 2 spans per step) for the same range of bandwidths. Again, we observe negligible improvement as we increase the bandwidth. The minimum Q-factor improvement that is observed is equal to ~0.3 dB and the maximum Q-factor improvement is equal to ~0.4 dB.

In Fig. 14, we show representative plots of the 2nd-order LPF-assisted IVSTF-NLE with 1-step-per-span and increasing bandwidth. Again, the Q-factor improvement doesn't exceed the ~0.5 dB as we increase the bandwidth.

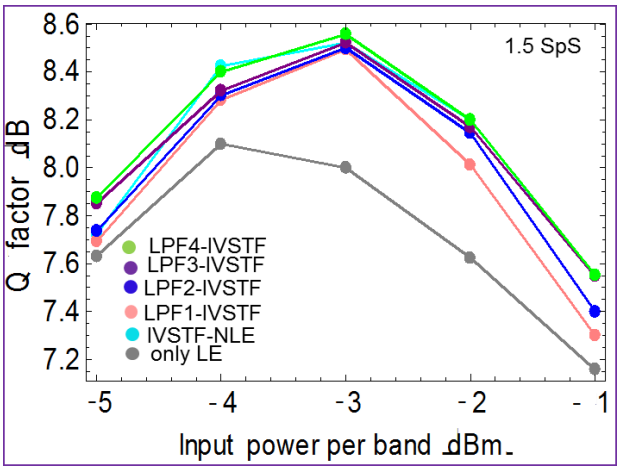

Fig. 12. Q-factor vs. input power per band without/with IVSTF-NLE and the 1st-order LPF-assisted IVSTF-NLE with single-step-per-span and increasing bandwidth in 3-channel, 4-band configuration after 10×100 km SSMF link.

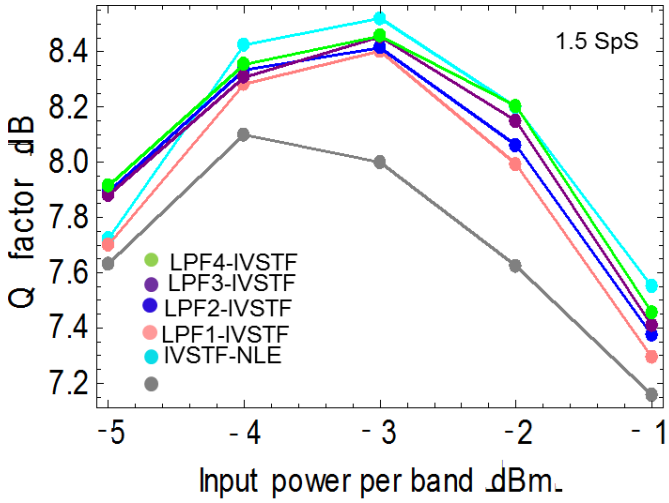

Fig. 13. Q-factor vs. input power per band without/with IVSTF-NLE and the 1st-order LPF-assisted IVSTF-NLE with 2 spans-per-step and increasing bandwidth in 3-channel, 4-band configuration after 10×100 km SSMF link.

Finally, in Fig. 15, we show representative plots of the Q-factor as a function of the input power per sub-band when applying the 2nd-order LPF-assisted IVSTF-NLE with 2 spans-per-step and increasing bandwidth. We observe that the maximum Q-factor improvement doesn't exceed ~0.35 dB.

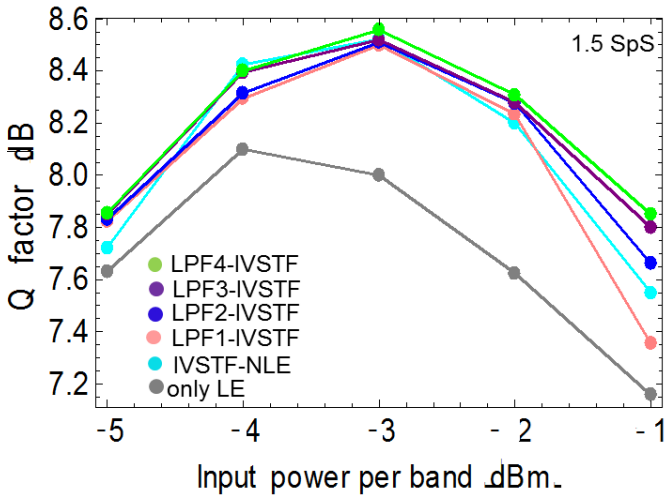

Fig. 14. Q-factor vs. input power per band without/with IVSTF-NLE and the 2nd-order LPF-assisted IVSTF-NLE with 1 step-per-span and increasing bandwidth in 3-channel, 4-band configuration after 10×100 km SSMF link.

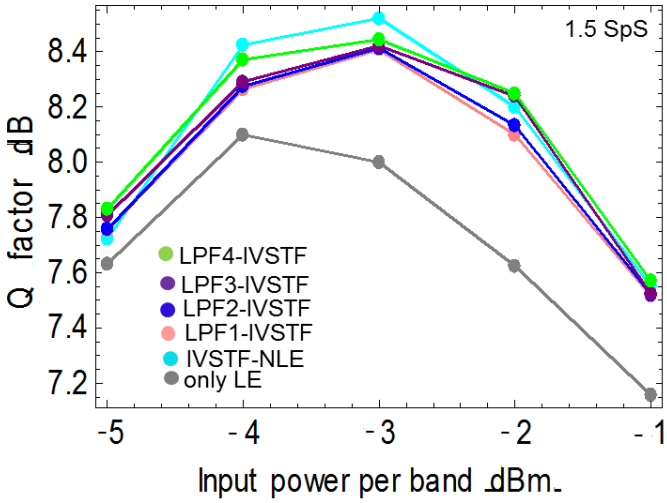

Fig. 15. Q-factor vs. input power per band without/with IVSTF-NLE and the 2nd-order LPF-assisted IVSTF-NLE with 2 spans-per-step and increasing bandwidth in 3-channel, 4-band configuration after 10×100 km SSMF link.

5.2.4 Performance investigation of the band-by-band and all-band equalization scheme of the IVSTF-NLE in single- and 3-channel, 4-band OFDM configuration

In this study case, we tested the performance of the IVSTF-NLE in two different equalization schemes:

1. Nonlinear compensation of only the central sub-band (band-by-band equalization scheme)
2. Nonlinear compensation of all the 4 sub-bands of the central channel (all-band equalization scheme).

The two equalization schemes are examined in the two scenarios, single-channel and 3-channel, 4-band OFMD.

In Fig. 16, we show the performance of the IVSTF-NLE in the single-channel transmission scenario by applying both equalization schemes (i.e. band-by-band and all-band).

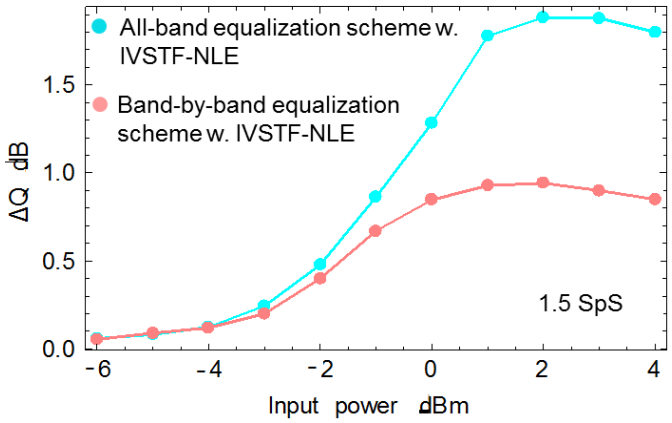

Fig. 16. ΔQ-factor improvement vs. input power per band without/with IVSTF-NLE in band-by-band and all-band scheme applied in 1-channel, 4-band configuration after 10×100 km SSMF link.

We observe that the all-band equalization scheme outperforms the band-by-band scheme by ~1 dB providing a Q-factor improvement equal to ~1.88 dB compared to linear case only. Similarly, in Fig. 17, we compare the performance of the band-by-band vs. all-band equalization scheme using IVSTF-NLE in 3-channel, 4-band OFDM configuration after 10×100 km.

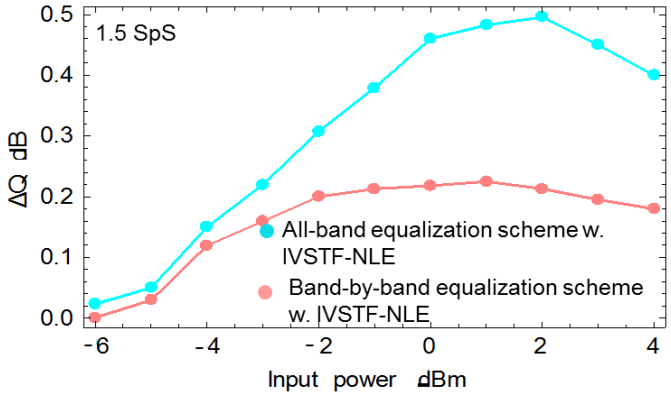

Fig. 17. ΔQ-factor improvement vs. input power per band without/with IVSTF-NLE in band-by-band and all-band scheme applied in 3-channel, 4-band configuration after 10×100 km SSMF link.

In this case, both equalization schemes exhibit modest performance with the band-by-band equalization scheme being only 0.2 dB inferior compared to all-band equalization scheme providing ~0.5 dB Q-factor improvement.

Finally, we test the IVSTF-NLE in the all-band equalization scheme for increasing number of sub-bands (i.e. 3, 5, 7 and 9 sub-bands) in the second scenario of nonlinearities in the 3-channel, 4-band OFDM configuration. In Fig. 18, we observe that as the number of sub-band increases the Q-factor improvement increases also and saturates at five sub-bands providing ~0.8 dB improvement compared to linear case only.

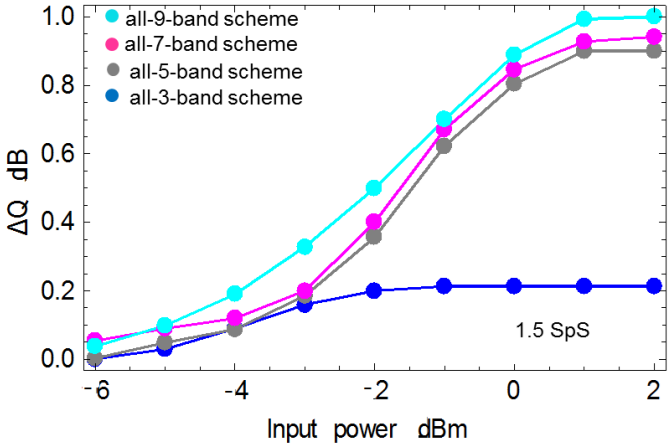

Fig. 18. ΔQ-factor improvement vs. input power per band without/with IVSTF-NLE in all-band scheme for increasing number of sub-band in a 3-channel, 4-band configuration after 10×100 km SSMF link.

5.2.5 Evaluation of computational complexity of the IVSTF-NLE, the single- and the 3-steps-per-span DBP-SSF

In this section, we compare the analytical IVSTF-NLE and the numerical equalizers DBP-SSF$_{Nsteps}$ in terms of computational complexity (i.e. number of real multiplications per polarization per sample) In Fig. 19, we have plotted the number of real multiplications as a function of the FFT block size for the DBP-SSF$_1$, the DBP-SSF$_3$ and the IVSTF-NLE equalizers for 10 spans. We observe that the DBP-SSF$_1$ and IVSTF-NLE differ only slightly in complexity while the DBP-SSF$_3$ appears to be almost three times more complex compared to the previous two.

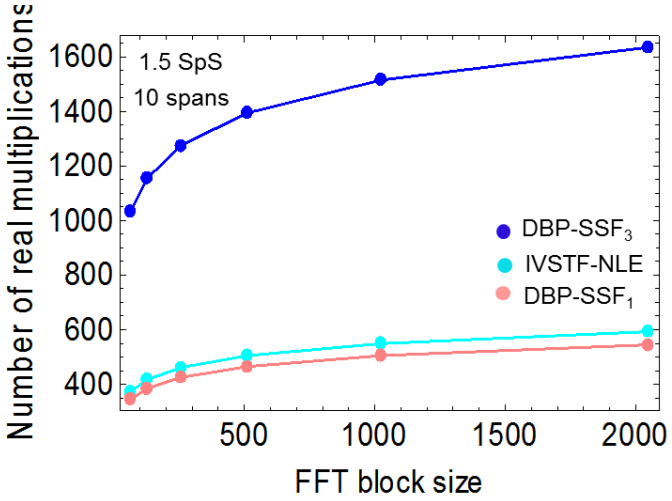

Fig. 19. Number of real multiplications per polarization per sample as a function of the FFT block size when applying the IVSTF-NLE, the DBP-SSF$_1$ and the DBP-SSF$_3$ equalizers after 10×100 km of SSMF.

5.2.6 Estimation of the power consumption considering a 45 nm ASIC technology

In this section, we assess via calculations the power consumed for the nonlinear compensation using IVSTF-NLE, the DBP-SSF1 and the DBP-SSF3 equalizers in a 32 Gbaud PDM-16QAM sub-channel. For all cases, the power consumption is estimated considering a 45 nm ASIC technology.

In Fig. 20, we show the power consumption of the aforementioned nonlinear equalizers compared to a linear one for transmission distances ranging from 100 to 1200 km.

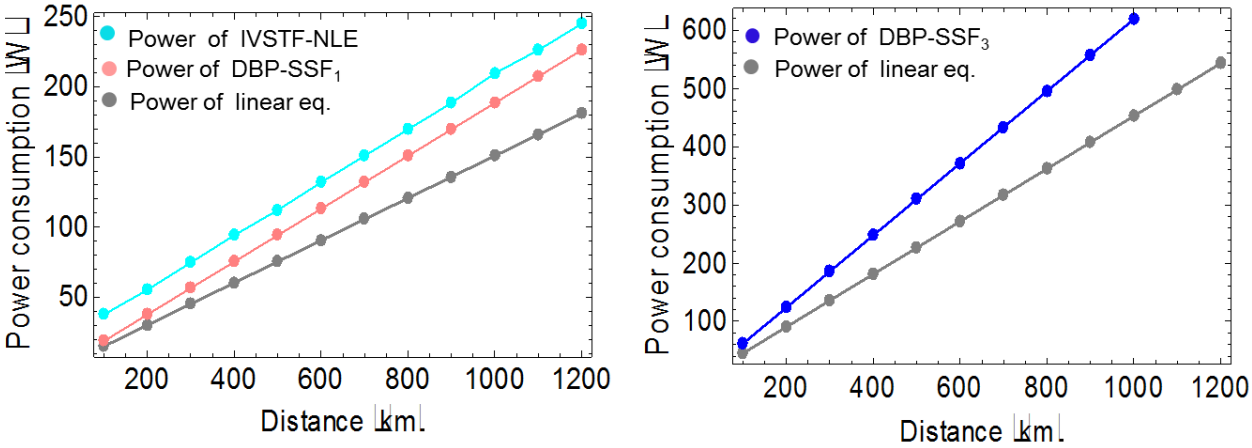

Fig.20. Power consumption as a function of the transmission distance for the IVSTF-NEL, the DBP-SSF$_1$ and the DBP-SSF$_3$ equalizers.

5.3 Conclusions

We compare via Monte Carlo simulations the performance of the 3rd-order IVSTF-NLE and DBP-SSF$_{Nsteps}$ in coherent single- and 3-channel, multiband OFDM configurations accommodating 400 Gb/s. All equalizer types offer almost identical performance, i.e. exhibiting a ~0.45 dB Q-factor improvement, compared to the linear equalization case, on the 3-channel, 4-band OFDM scenario. As a second step, we compare the nonlinear equalizers in terms of computational complexity. We observe that the IVSTF-NLE and the DBP-SSF$_1$ have almost similar computational complexity with the latter being only slightly less complex. Compared to DBP-SSF$_3$, the IVSTF-NLE is almost three times less complex. In terms of power consumption, the IVSTF-NLE consumes ~21.770 W more power compared to the DBP-SSF$_1$. On the contrary, the DBP-SSF$_3$ consumes 409 W more power than the IVSTF-NLE. Thus, IVSTF-NLE

could be a reasonable choice as a first-generation nonlinear equalizer at relatively low implementation complexity.

In an effort to fully investigate the potential of the 3rd-order IVSTF-NLE, we also studied, via numerical simulations, a few variants of the original version. However, the results were not encouraging. More specifically, we show that the multistep-per-span IVSTF-NLE and the LPF-assisted IVSTF-NLE don't provide any further Q-factor improvement compared to the conventional IVSTF-NLE.

Finally, we tested the 3rd-order IVSTF-NLE in the all-band equalization scheme by increasing the number of sub-bands. We observed that by increasing the number of sub-bands of the central channel from 3 to 9, the provided Q-factor improvement does increase reaching almost 1 dB compared to the case of linear equalization only.

References for section 5

[1]. L. Liu, L. Li, Y. Huang, K. Cui, Q. Xiong, F.N. Hanske, C. Xie and Y. Cai, "Intrachannel nonlinearity compensation by inverse Volterra series transfer function," *J. Lightw. Technol*., vol. 21, no. 3, pp. 310-316, Feb. 2012.

[2]. E. Ip and J. M. Kahn, "Compensation of dispersion and nonlinear impairments using digital backpropagation," *J. Lightw. Technol*., vol. 26, no. 20, pp. 3416-3425, Oct. 2008.

[3]. S. J. Savory, "Digital filters for coherent optical receivers", Opt. Exp., vo. 16, no. 2, pp. 804-817, Jan 2008.

[4]. G. P. Agrawal, *Fiber-optic communication systems*, 3rd ed. New York, NY, USA: Wiley, 2003.

[5]. Y. Gao, J. H. Ke, K. P. Zhong, J. C. Cartledge and S. S. –H. Yam, "Assessment of intrachannel nonlinear compensation for 112 Gb/s dual-polarization 16QAM systems," *J. Lightw. Technol*., vol. 30, no. 24, pp. 3902-3910, Dec. 2012.

6. AO-OFDM transmission experiments

In this section, the experimental demonstrations of the all-optical OFDM approach developed within ASTRON are described. The basic principle of all-optical OFDM is very similar to the implementation of the digital discrete Fourier transform/inverse digital discrete Fourier (DFT/IDFT) used in conventional OFDM schemes. A short optical pulse train is generated by either a mode-locked laser diode (MLLD) or a comb source at the transmitter (TX), and the optical spectrum is composed of a set of lines spaced at the symbol rate. A splitter equally divides the input power into a set of optical signals, that are individually modulated by optical modulators and *sinc*-shaped filtered, as shown in Fig. 21 (a). This scheme is referred to as AO-OFDM architecture in the ASTRON project. Either an array waveguide gratings (AWG) [1], a wavelength selective switch (WSS) [2], or both [3] can be used as optical filter and (de)multiplexer; in the first case, different functionalities can be integrated on the same platform, and there is no power dissipation. On the other hand, a WSS can be suitably programmed, introducing bandwidth flexibility.

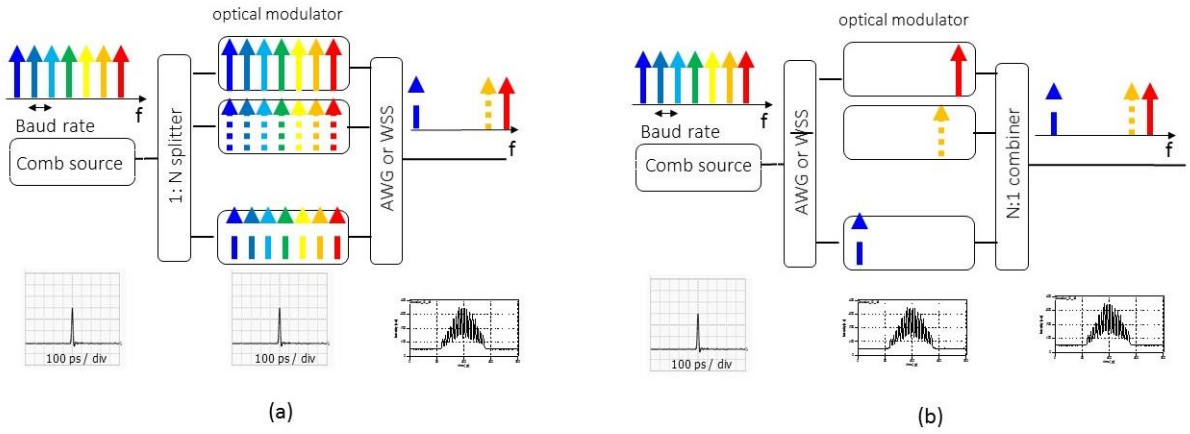

Fig. 21. Complementary schemes of an optical OFDM transmitter. (a) AO-OFDM (b) OS-OFDM.

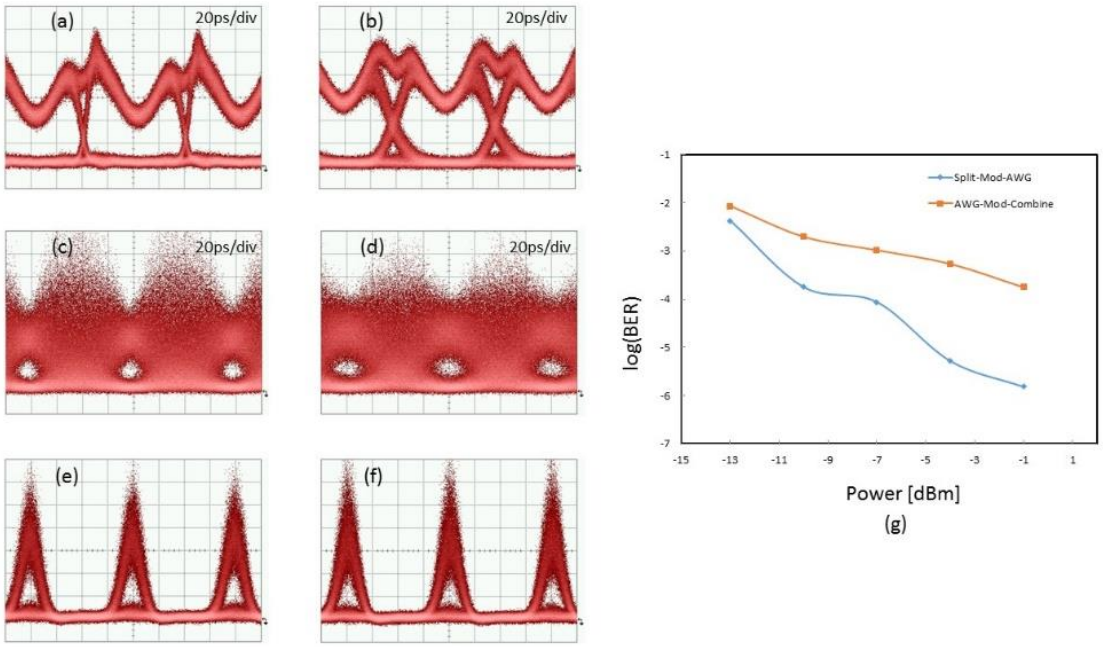

Fig. 22. (a) AO-OFDM symbol (b) OS-OFDM symbol. (c) AO-OFDM demultiplexed signal (d) OS-OFDM demultiplexed signal. (e) AO-OFDM signal after time gating (f) OS-OFDM signal after time gating. (a), (c) and (e) are obtained with the AO-OFDM TX of Fig. 21(a) and (b), (d) and (f) with the OS-OFDM scheme of Fig. 21(b). (g) BER performance of the AO-OFDM and OS-OFDM schemes of Fig. 21.

A complementary OFDM TX architecture is shown in Fig. 21(b), where the position of the splitter and optical multiplexer are inverted, compared to Fig. 21(a). This approach is referred to as OS-OFDM configuration in the ASTRON project. In this case, the input optical lines are demultiplexed and shaped by the AWG or the WSS, that generate the OFDM symbols. A detailed analytical and numerical comparison of the two approaches is presented in Refs. [4, 5], showing that the system performance in the configuration of Fig. 21 (b) strongly depends on the digital analog converter (DAC) and modulator bandwidth, which affects the subcarriers orthogonality of the subcarriers.

Roma3 and the Photonic Network System Laboratory of the National Institute of Information and Communications Technology (NICT) Japan, have performed a basic experiment that confirms this result. We considered a 16 subcarrier, 12.5 GHz spaced optical OFDM system, using Lithium Niobate

phase modulators, with approximately 12.5 GHz bandwidth. The OFDM symbol corresponding to a single subchannel is shown in Fig. 22 (a) and (b), using the AO-OFDM and OS-OFDM architectures of Fig. 21, respectively. In the case of the AO-OFDM setup of Fig. 21(a), the rising and falling time is about 40 ps, and it is related to the input pulse duration. On the other hand, using the OS-OFDM setup of Fig. 21(b), the symbol rising and falling time becomes 40 ps, due to 12.5 GHz modulator bandwidth. We incidentally observe that in both cases the OFDM symbols do not have a rectangular profile, due to an additional waveform reshaper, that has been introduced after the TX, to enhance the system performances and compensate the slab diffraction effect in the AWG [6]. At the receiver (RX) side, the signal is first demultiplexed using another AWG, or a WSS and then time gating is applied. The demultiplexed signal, before and after time gating are shown in Fig. 22(c) and (e), respectively, for the AO-OFDM setup of Fig. 21(a), and in Fig. 22(d) and (f), for the OS-OFDM setup of Fig. 21(b). Finally the BER measurements of Fig. 22 (g) confirm that the scheme of Fig. 21(a), is suitable to reduce the interchannel interference (ICI), thanks to the steep rising and falling edge of the OFDM waveforms. Therefore, we can conclude that the AO-OFDM scheme of Fig. 21(a) is the most favourable, thanks to the short duration of the modulated optical pulses, that are not affected by the electrical waveform, modulator bandwidth, or DAC resolution. Therefore, ROMA3 and NICT have investigated only the AO-OFDM configuration of Fig. 21(a) [7].

A complete theoretical and numerical analysis of the AO-OFDM configuration and performance has also been carried out during the first period of the ASTRON project [8-17].

6.1 Multiplexer/demultiplexer

Both a WSS and an AWG can be used to optically (de) multiplex the subchannels, using *sinc*-shaped filters [3]. At the TX, to reduce interchannel interference (ICI) without affecting other system performance, we apply a filter function that eliminates all the sidelobes of the *sinc*-function, as shown in Fig. 23.

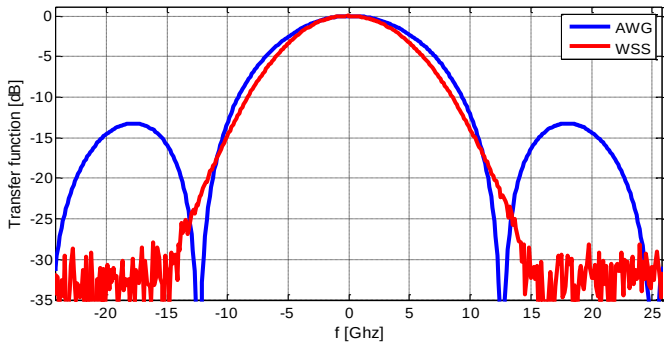

Fig. 23 Measured WSS transfer function and numerical simulation of the AWG transfer function.

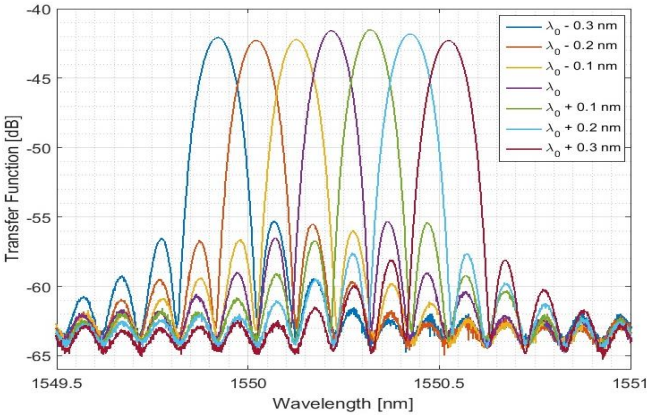

Fig. 24 Measured 7-channel spectra at the AWG outputs

In our experiment, we programmed a WSS with a second-order super-Gaussian shape; the 3dB and 6dB bandwidths are 9.8 GHz and 13 GHz, respectively. The numerically simulated AWG transfer function is also shown for reference in Fig. 23. The proposed system largely reduces the overall ICI when optical time gating is not applied and chromatic dispersion (CD) is not compensated. The use of a WSS in the TX allows bandwidth management flexibility, as different subcarriers can be easily assigned by programming the WSS. On the other hand, only an AWG can generate a *sinc*-shaped filter with high resolution, and demultiplex a large number of AO-OFDM subcarriers. Therefore, at the RX, we used an AWG to simultaneously demultiplex all the subchannels, and Fig. 24 reports the measured spectra at the AWG outputs.

6.2 AO-OFDM PON: description of the laboratory test bed

An experimental testbed for AO-OFDM systems was set at NICT's Laboratories, using both direct detection with differential phase shifted keying (DPSK) and differential quadrature phase shifted keying (DQPSK) modulation, and coherent detection with QPSK modulation. Seven-user, 12.5 Gbaud/user transmission was demonstrated over 40 km of single mode fiber, to increase data rate in next generation optical access networks, overcome the TDM limitations and enhance the spectral efficiency.

To optically generate the AO-OFDM subcarriers, a flat and stable optical comb is needed, to ensure orthogonality of the channels. The comb was generated using a single light source, a dual-drive Mach-Zehnder modulator (DD-MZM), and an optical phase modulator (PM); a WSS is used at the TX to optically shape the input light source with a frequency *sinc*-like profile, and generate the AO-OFDM subcarriers.

Fig. 25 shows the experimental TX setup for a 7- user DQPSK-modulated AO-OFDM system; the subcarrier spacing equates to the symbol rate B=12.5 GHz, to achieve the maximum spectral efficiency. The optical comb is generated by a tunable laser diode (TLD) centered at 1550.259 nm, followed by a DD-MZM, an

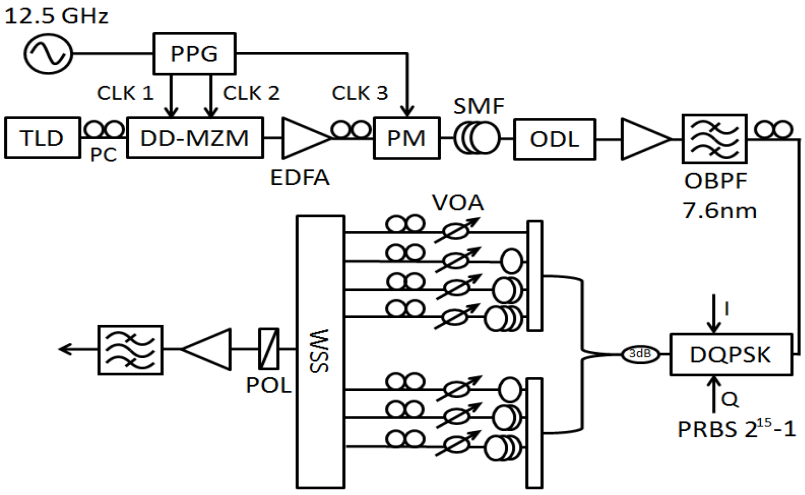

Fig. 25 Transmitter setup. Tunable laser diode (TLD), polarization controller (PC), dual-drive Mach-Zehnder (DD-MZM), pulse pattern generator (PPG), erbium-doped fiber amplifier (EDFA), clock (CLK), phase-modulator (PM), single mode fiber (SMF), optical delay line (ODL), optical band pass filter (OBPF), differential quadrature phase shift keying (DQPSK) modulator, variable optical attenuator (VOA), wavelength selective switch (WSS), polarization scrambling (POL), pseudo random bit sequence (PRBS).

optical PM and a single mode fiber (SMF) that compresses the optical pulse. The two cascaded modulators are driven both at B=12.5 GHz. The peak to peak voltages at the outputs of the two RF driver amplifiers of the DD-MZM are 8.3 V and 11 V; the PM is driven by a signal with 5.6 V peak to peak, to increase the overall modulation index. In our experiment, the comb is composed of seven lines with power fluctuation less than 1.9 dB as shown in Fig. 26(a): the train of Gaussian pulses shown in Fig. 26(b) has 13-ps FWHM. After the PM modulator, a 3-km SMF is used for pulse compression, an optical delay line (ODL) synchronizes the optical pulse peak with the electrical signal; and an erbium-doped fiber amplifier (EDFA) and an optical band pass filter (OBPF) are employed. A DQPSK transmitted signal is obtained by precoding two 2^{15}-1 pseudo random data sequences (PRBS) for the in-phase (I) and quadrature (Q) signals, that are sent to a pulse pattern generator (PPG). All the optical comb lines are modulated by the same electrical signal, and the seven subcarriers are generated using a 3 dB coupler followed by two 6 dB couplers; variable optical attenuators (VOA) are used to equalize the subcarriers power, polarization controller (PC) and delay lines are used to decorrelate the seven optical signals. The lengths of the decorrelation delay lines are 1, 2, 3, 4 and 5 m. In this way, we can achieve a fully subcarrier decorrelation and no ICI underestimation.

A 1x8 WSS with 6 dB insertion loss is used at the TX; the measured transfer function for seven subcarriers is shown in Fig. 27. After the WSS we use a polarization scrambling (POL), an EDFA and a 7.6-nm OBPF. The total launched power to the SMF is 2 dBm.

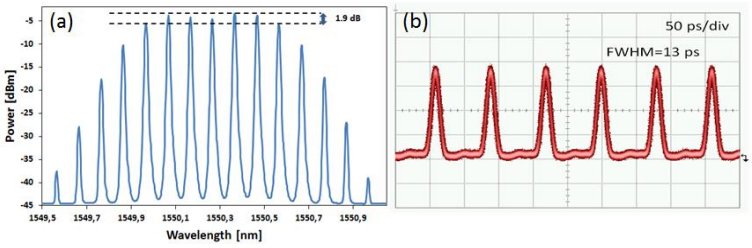

Fig. 26. (a) Measured optical comb. (b) Measured Gaussian pulses.

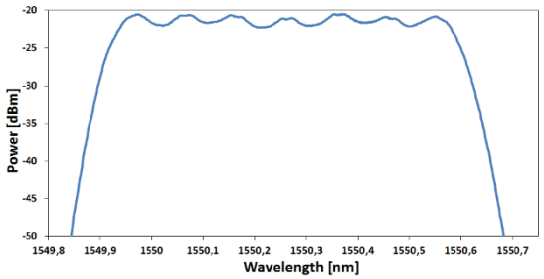

Fig. 27. Measured optical spectrum at the WSS output.

Figure 28 shows the RX setup which consists of a VOA and a 20-dB coupler before the AWG in order to measure the received power with a power meter (PWM). The AWG has 16 ports, 200 GHz free spectral range (FSR), 12.5 GHz subcarrier spacing and 10 dB insertion loss. We use a pre-amplifier, a 7.6-nm OBPF, a one-bit delay line interferometer (DLI) and a balanced photo-detector (BPD), with 45 GHz bandwidth, to measure the bit error rate (BER). The BER tester (BERT) supports line rates up to 32 Gb/s.

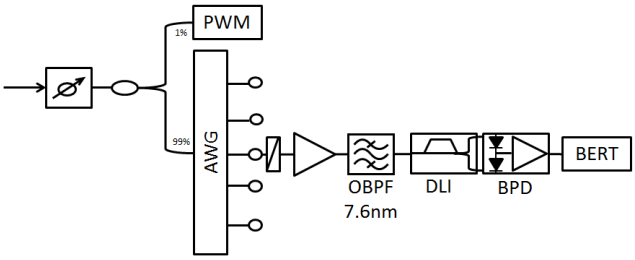

Fig. 28. Receiver setup. Power meter (PWM), arrayed waveguide grating (AWG), delay line interferometer (DLI), balanced photodetector (BPD), bit-error rate tester (BERT).

We have extended our analysis considering also a fiber Bragg grating (FBG) at the RX, to filter the AO-OFDM signal [18, 19]. An AWG or WSS are used to (de)multiplex all the subcarriers in parallel; on the other hand, a FBG selects only one subcarrier from the received signal. The use of a FBG is advantageous to reduce the costs in optical access networks. Fig. 29 shows the experimental setup for three 12.5 Gb/s DPSK modulated subcarriers. The TX is same as that of setup in Fig. 25; at the RX side a FBG is used, with a *sinc*-shaped transfer function to filter a single AO-OFDM subcarrier, with 20 dB insertion loss. A VOA is used to vary the received optical power after the FBG.

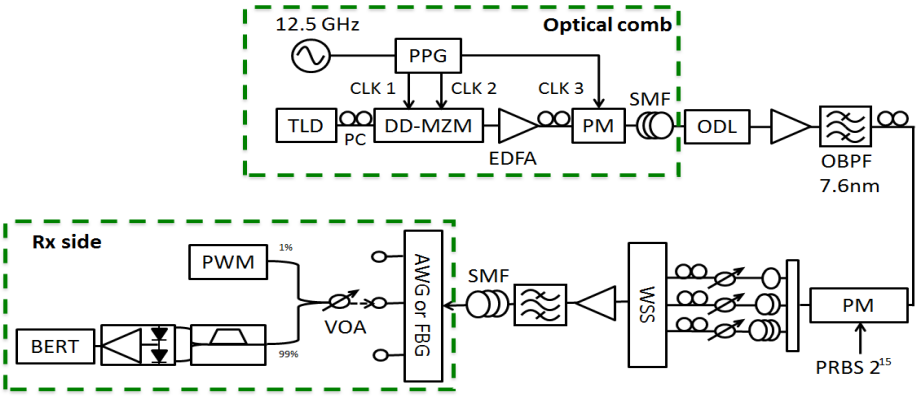

Fig. 29 Experimental setup of an AO-OFDM system using either AWG and FBG at the receiver.

6.3 AO-OFDM PON system: measured performance

The measured eye diagrams of a seven channel B2B system, and after 35-km SMF are reported in Fig. 30(a) and 5.10(b), respectively; no optical time gating or CD compensation have been used. Fig. 31(a) reports the received spectrum at an AWG output port, for a transmission of seven AO-OFDM subcarriers, and Fig. 31(b) refers to the case when the target subcarrier is not transmitted, i.e. measures the ICI at the same port from the other six carriers. The measured crosstalk is -35.6 dBm.

Fig. 32 reports the BER measurements as a function of the total received power. The B2B behavior is compared with the performance obtained with the same setup, using QPSK modulation and coherent detection.

In case of coherent detection, five adjacent subcarriers, spaced 12.5 GHz each, are taken into account. DQPSK-modulated subcarrier in B2B presents about 3-dB penalty at BER=10^{-6} with respect to coherent detection.

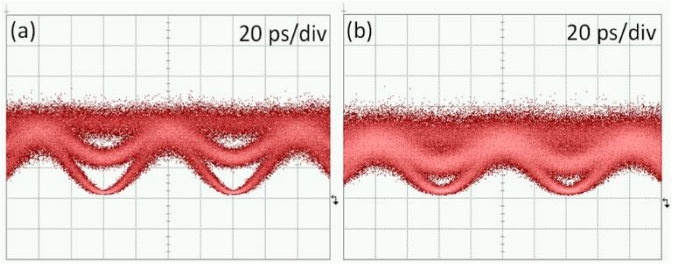

Fig. 30. Measured eye diagrams of a 7 channel transmission (a) B2B (b) after 35-km SMF.

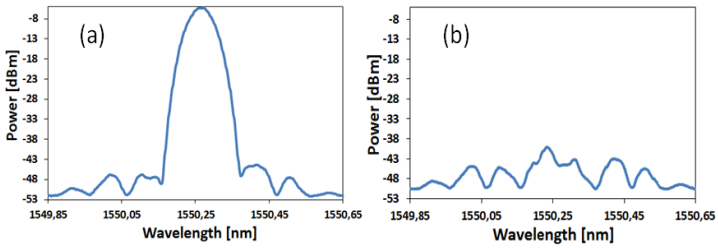

Fig. 31. Spectrum measured at an AWG output port (a) transmitting seven AO-OFDM carriers (b) transmitting six subcarriers (the target subcarrier has been switched off).

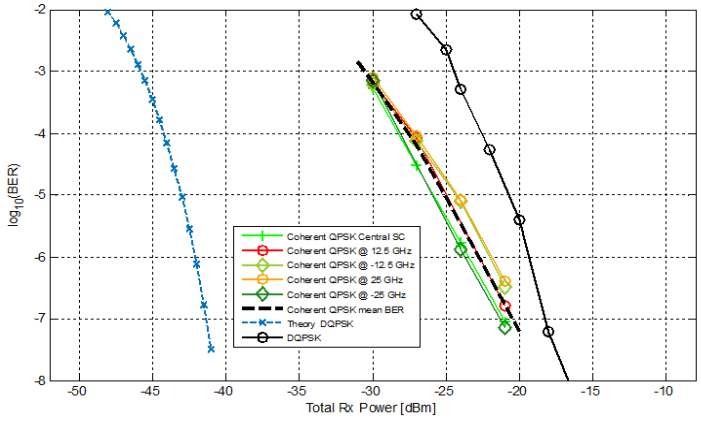

Fig. 32. BER vs received power in BTB for a DQPSK-modulated subcarrier received with direct detection compared with five QPSK subcarriers received by coherent detection (the dashed line corresponds to the mean BER curve of the five subcarriers). A theoretical curve for direct detection is also shown for reference.

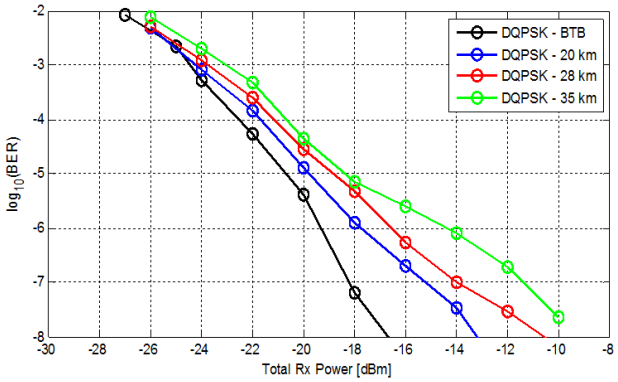

Fig. 33. BER vs received power for a DQPSK-modulated subcarrier for B2B, 20-km, 28-km, and 35-km transmission over uncompensated SMF.

Figure 33 reports BER measurements after 20-km, 28-km and 35-km SMF for single DQSPK modulated subcarrier, without any dispersion compensation. Error-free transmission is achieved for all the subcarriers.

Referring to the setup of Fig. 29, we report the results by comparing the FBG and AWG demultiplexing performance in terms of BER as a function of the received optical power.

Figure 34(a) reports the BER measurements as a function of the total received power, when a FBG is used at the RX to extract a single optical subcarrier. The red line refers to the case when only one subcarrier is transmitted in a back-to-back (B2B) setup. In this case, the received optical power for log(BER) =-4 is -17.5dBm. The blue line reports the system performance when two adjacent subcarriers are transmitted in a B2B configuration. From a comparison, we observe that the ICI penalty is 1.5 dB at log(BER) =-4.

Adding another subcarrier in the B2B setup, an error floor is reached for log(BER)=-8.3 due to ICI and the high loss of the FBG (see green curve).

Two and three AO-OFDM subcarriers have been transmitted over 40km SMF. In case of two subcarriers (black curve), error free transmission was achieved, with a penalty of 2.5dB respect to B2B case.

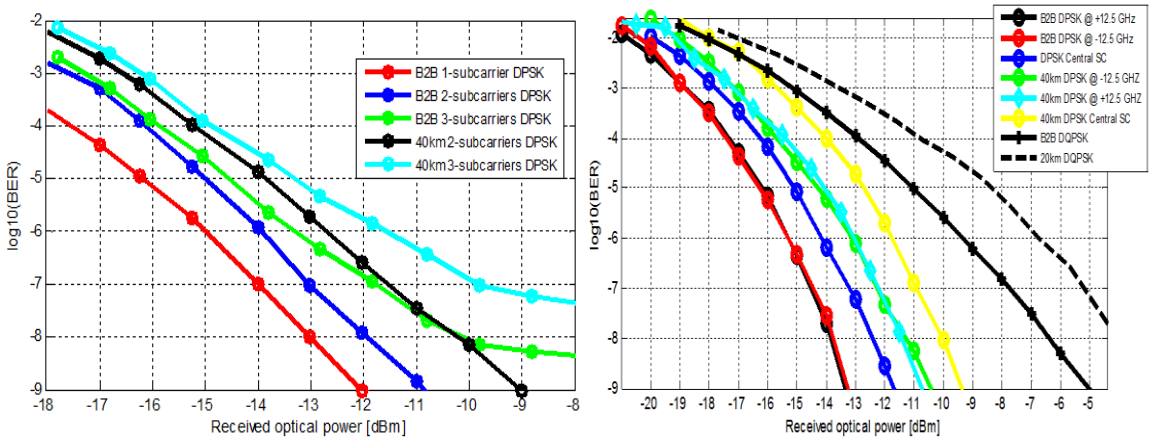

(a) (b)

Fig. 34 (a) BER vs. received optical power for DPSK modulated subcarriers, when a FBG is used at the ONU RX side, (b) BER vs. received optical power for DPSK and DQPSK modulation, when an AWG is used at the remote node.

The same penalty is observed transmitting three subcarriers (cyan curve), but in this case an error floor for log(BER) = -7.3 is achieved.

Figure 34(b) shows the performance of the same system, using an AWG at the RX. In this case, we have used either DPSK or DQPSK modulation. In the latter case, the PM in the TX has been replaced by an I/Q modulator with same PRBS. The blue line refers to the DPSK modulation and B2B case, for the center subcarrier, black and red lines to the other two adjacent subcarriers. As expected, the center subcarrier presents a 1 dB penalty compared to the other two subcarriers, for log(BER)= -4.

Also in this case, we have tested the system performance by transmitting over a 40km-long SMF. The adjacent subcarriers (green and cyan curves) present about 1.3 dB penalty with respect to the B2B case. For the center subcarrier (yellow curve), the penalty is 2.2 dB. However, in all case, the BER does not present any floor and error-free transmission has been demonstrated using an AWG at the RX remote node. Finally, the last two black curves refer to DQPSK modulation, in B2B and after 20 km SMF; in this case the power penalty after transmission is 1.3dB for log(BER)= -4.
In conclusion, ROMA3 and NICT have experimentally demonstrated that:

1. AO-OFDM system can be used in long-reach access networks, allowing high data rates per user up using both direct detection and complex modulation formats. System performances of five subcarrier with coherent detection and seven subcarrier with direct detection have been experimentally investigated.
2. To enhance the system performance, we used a WSS at the TX and an AWG at the RX. The DFT/IDFT is optically implemented and the Digital signal processing (DSP) is reduced, compared to electrical OFDM systems, and no digital to analog converter (DAC) is required at the TX.
3. The optical distribution network (ODN) losses of 22dB can be supported with direct detection and 25dB with coherent detection.
4. AWG outperform the FBG performance, presenting lower losses.

6.4 Hybrid OFDM PON: description of the laboratory test bed

In the previous paragraphs AO-OFDM has been demonstrated to be a promising approach for next generation high-capacity PONs, thanks to the implementation of the IFFT/FFT operation directly in the optical domain by means of passive and energy efficient AWGs. AO-OFDM appears particularly

interesting for the downstream transmission as, at the PON remote node (RN), the AWG can be exploited to optically demultiplex the OFDM subcarriers before the optical network unit (ONU) detection. On the other hand, AO-OFDM requires a complex transmission stage, based on a stable and flat comb generator, necessary to provide subcarriers orthogonality.

In the ASTRON project, we proposed also a hybrid OFDM approach, based on electronic DSP at the optical line terminal (OLT) to generate the OFDM signal and on all-optical FFT processing and demultiplexing at the RN. This solution guarantees drastic simplicity for the PON implementation, increased by the choice of the OOK modulation format for the OFDM subcarriers, which allows to exploit the direct detection at the ONU. In this way, the hybrid OFDM can maintain the advantages of AO-OFDM for future PONs, exploiting the whole available transmission spectrum together with a fine granularity in the subcarriers assignment with dynamic bandwidth access. At the same time, the hybrid OFDM assures reduced complexity and cost in the realization.

ROMA3 and NICT have analyzed the hybrid OFDM architecture reported in Fig. 35 [20-22]. We employed multi-wavelength sources emitting 50-GHz spaced carriers, with each optical carrier separately modulated at the OLT by a hybrid OFDM transmitter block, generating a 37.5-Gb/s 3-subcarrier OFDM signal. The experimented aggregate bit rate and subcarrier configuration is due to two constraints: the availability of state of the art AWG components operating as FFT block with a frequency spacing between the demultiplexed neighbour OFDM subcarriers of 12.5 GHz and the limitations of the available DSP and digital-to-analog converters (DACs) necessary at the OLT to generate in the electrical domain the OFDM signal. Both constraints forced us to assume to have the availability of a maximum of three OFDM subcarriers, each modulated at 12.5 Gbaud. In case of OOK modulation, each OFDM transmitter block thus offers 12.5-Gb/s data to each ONU, corresponding to a specific OFDM subcarrier, assuring 37.5-Gb/s aggregate downstream capacity per wavelength.

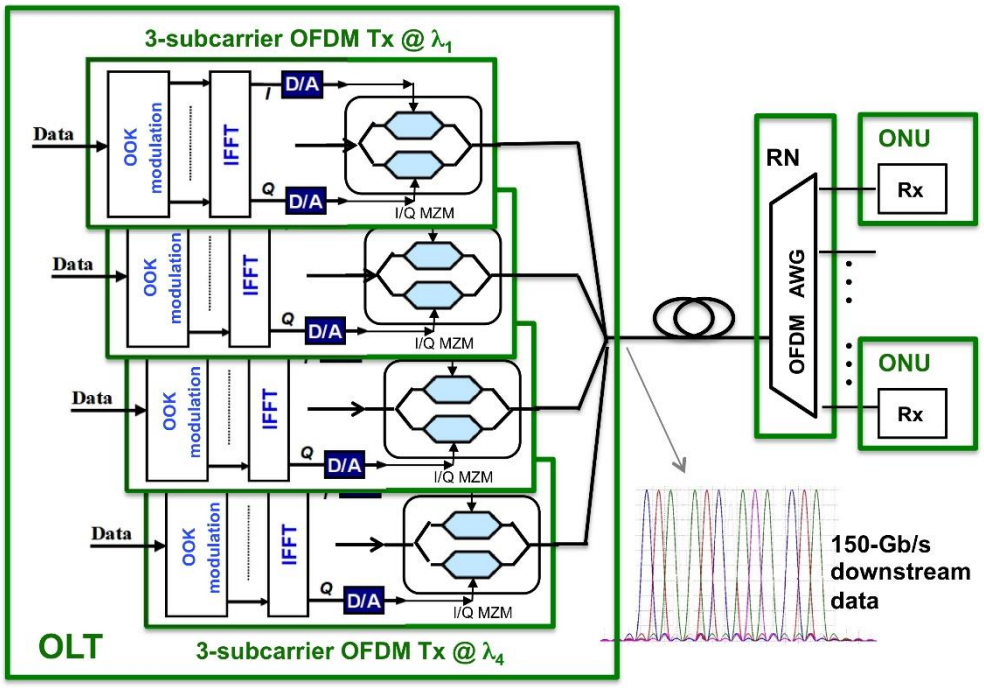

Fig. 35: PON network based on the hybrid OFDM solution in case of 16-port OFDM AWG exploitation.

After modulation, the OFDM subcarriers coming from the multi-wavelength sources are aggregated by a simple coupler and transmitted via the feeder link. At the RN a single AWG is employed to demultiplex in an all-optical and passive way the OFDM subcarriers. Given that the experimented AWG has 16 ports

and supposing to maintain a 12.5-GHz guard band between the OFDM subcarriers coming from adjacent wavelength carriers, 4 different 3-subcarrier OFDM signals can be FFT-processed and demultiplexed at the same time by the AWG. The proposed PON can thus accommodate 12 ONUs achieving a total 150-Gb/s aggregate downstream capacity. The whole downstream capacity and the number of served ONUs can be easily enhanced by increasing the number of output port of the employed AWG and consequently the number of optical carriers.

Fig. 36 presents the experimental test bed employed to demonstrate the behaviour of a single 37.5-Gb/s OFDM transmitter block. The experimental test bed was set up at the Lab of the New Generation Network Research Center of NICT, which supported the ASTRON research by hosting in NICT Labs young researchers from ROMA3 and making available advanced instrumentations and devices for ASTRON experimentation. The OFDM signal with three 12.5-Gb/s OOK modulated subcarriers was electronically generated through DSP and DACs by means of a pair of synchronous Tektronix arbitrary waveform generators 70001A operating with 50-GS/s sampling rate. They fed the real and imaginary components of the signal to the I and Q arms of a nested Mach-Zehnder modulator (MZM). The parallel OFDM symbols were generated through the DSP in the IFFT block. The DSP generation provided full OFDM subcarriers decorrelation, avoiding inter-carrier interference (ICI) underestimation. No cyclic prefix was inserted in the OFDM signal.

After the propagation over SSMF, at the RX side, the tailored 16-port AWG was used as a passive and all-optical OFDM subcarrier demultiplexer with 12.5-GHz frequency spacing and 200-GHz FSR, performing the FFT operation. Thus, the demultiplexed and demodulated subcarriers were output at the corresponding AWG ports, which were then linked to the ONU user receivers. As each subcarrier was OOK-modulated, a direct detection (DD) scheme was applied at the receiver.

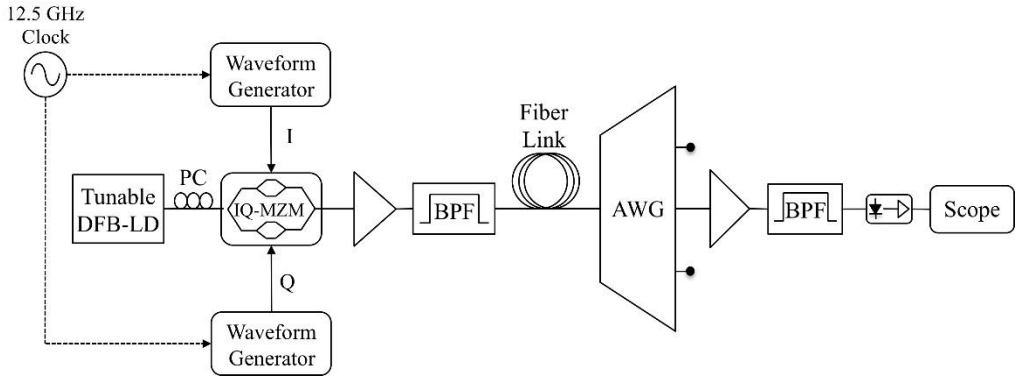

Fig. 36. The experimental set up.

6.5 Hybrid OFDM PON system: measured performance

Fig. 37 (a) shows the optical spectrum of the 3x12.5-Gb/s OFDM signal per wavelength generated by the pair of arbitrary waveform generators and measured after the MZM by means of an optical spectrum analyser. Owing to the limited bandwidth of the arbitrary waveform generator, the external subcarriers are more penalized with respect to the inner subcarrier during the electro-optical generation. In Fig. 37 (b), (c) and (d) the spectra at the output ports of the AWG are reported. The effect of the demultiplexing and the filtering of the subcarriers is visible and presents a good extinction ratio.

Fig. 38 shows the system performance in terms of bit error rate (BER) evaluated in back-to-back (BTB) and after propagation over 20 km and 40 km SSMF, typical reach of PONs. After 20-km SSMF, about 4-dB penalty is present at 10^{-4} BER with respect to BTB, while after 40-km SSMF the penalty goes up to

almost 8 dB, due to the increasing effect of chromatic dispersion for 12.5-Gb/s OOK subcarrier modulation. No cyclic prefix is inserted in the OFDM signal. We have performed dispersion compensation by exploiting a reverse dispersion fibre (RDF) after 40-km propagation, obtaining a strong performance improvement and BER values comparable with the BTB case.

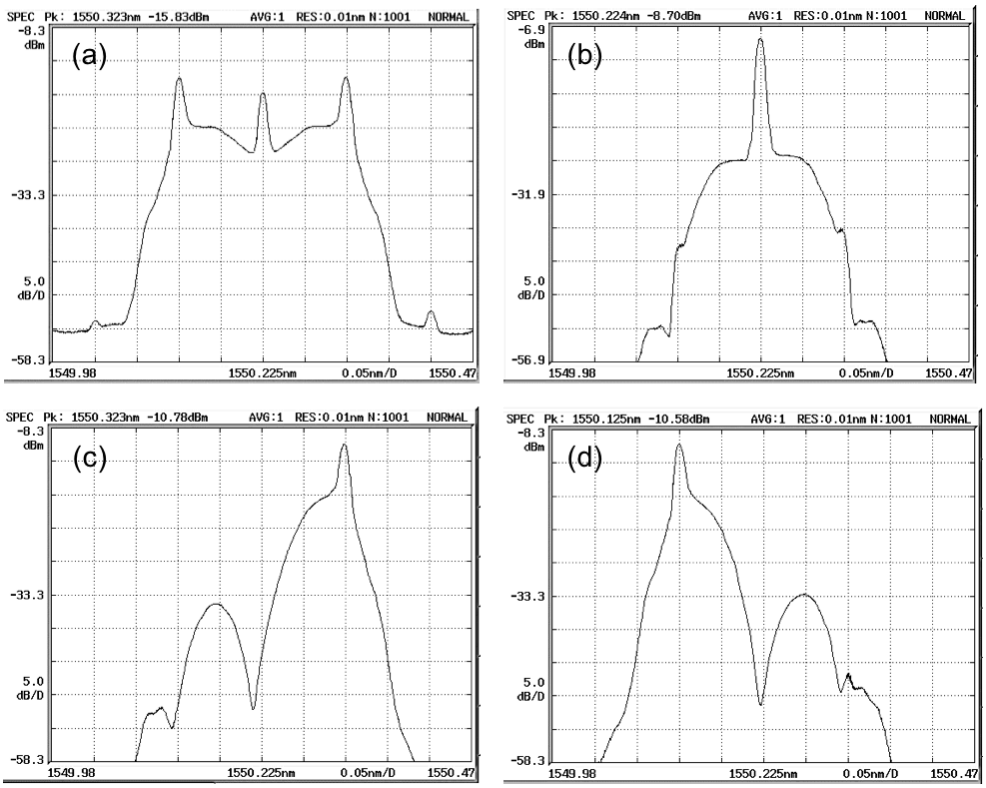

Fig. 37. Spectrum of the 3x12.5-Gb/s OFDM signal before the AWG (a). Spectra at the AWG output ports corresponding to the selected inner subcarrier (b), and the selected external subcarriers (c) and (d).

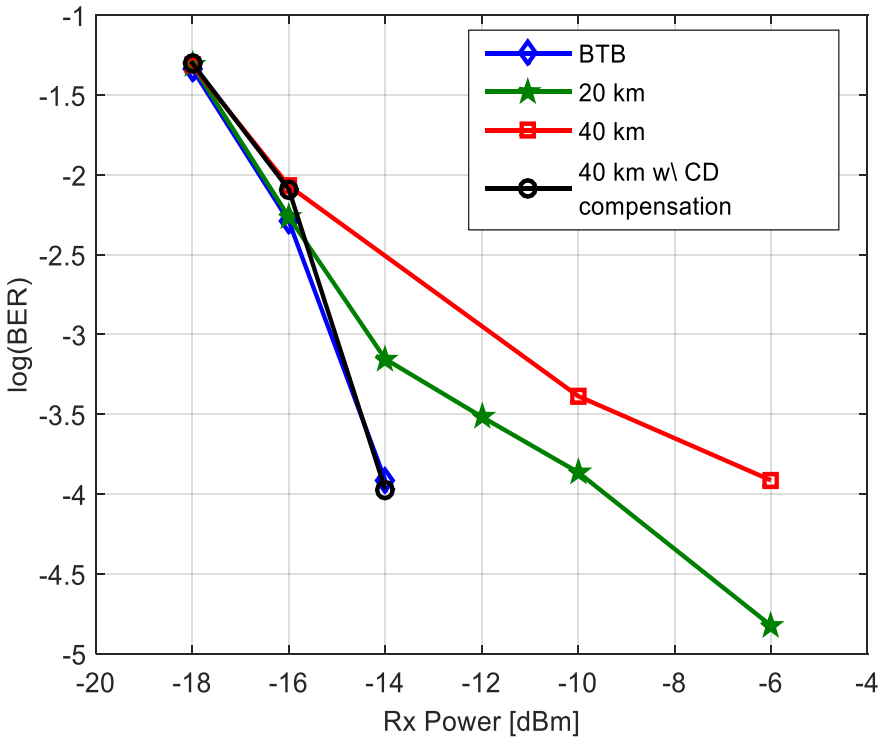

Fig. 38 Experimental measured BER vs. received power per subcarrier in case of 3x12.5-Gb/s OOK hybrid OFDM system in case of BTB (blue line), 20-km SSMF propagation (green line) and 40-km SSMF propagation (red line). The black line represents the BER performance when a RDF is employed after 40-km SSMF propagation to compensate for the chromatic dispersion.

In conclusion, the transport of a 37.5-Gb/s aggregate OFDM signal over more than 40-km reach has been demonstrated in ASTRON project by exploiting also a hybrid solution based on the electrical generation of the OFDM signal and on the all-optical and passive subcarrier demultiplexing implemented by the AWG. Performance evaluation in terms of BER has been performed by exploiting the 16-port AWG developed by the Japanese CNIT Research Center to optically implement the FFT operation. Low complexity and cost at the ONU were obtained by adopting OOK modulation for each subcarrier. A downstream capacity of 150-Gb/s is achievable by exploiting the proposed PON solution in presence of four DFB sources with 50-GHz channel spacing, but it can be easily increased by exploiting a RN AWG with a larger port number.

7. OFDM-OTDM transmission experiments

OFDM and Nyquist-optical time division multiplexing (N-OTDM) are alternative approaches to generate Tb/s superchannels, multiplexing subcarriers in frequency, or interleaving short *sinc*-shaped pulses in time. Both methodologies have pros and cons, mainly related to physical impairments and implementation issues. For instance, OFDM is more resistant to linear effects, such as CD, since the transmitted symbol is stretched in time, but, with an increased peak-to-average power ratio (PAPR), it becomes more sensitive to nonlinear effects. In general when selecting a time or frequency multiplexing approach, a trade-off is achieved, sacrificing spectral efficiency to a higher capacity, or system performances to a reduced complexity. The ultimate efficiency in physical resource exploitation can be achieved only in truly flexible systems, where it is possible to switch from time to frequency multiplexing and vice versa, through intermediate grids.

The use of fractional Fourier transform (FrFT), instead of conventional Fourier transform (FT) subcarriers, allows us to introduce the largest degree of flexibility in optical networking, moving from time to frequency multiplexing and viceversa. OFDM and N-OTDM systems are implemented by the same TXs, and have different RXs. In the TX, AWGs or WSSs are used as waveshapers. The proposed

approach introduces ultimate flexibility allowing us to receive either OFDM subcarriers in parallel or a serial N-OTDM signal.

Roma3 has already demonstrated the record generation of 4.88 ps sinc-shaped N-OTDM pulses, using the same WSS-based TX, and a dispersion compensating fiber (DCF) [23, 24]; the WSS induces a quadratic phase modulation (QPM) on an input pulse, and the time-lens effect in the DCF compresses, properly shapes and delays the sinc pulses to generate a N-OTDM signal.

In collaboration with the STARBOARD project, Roma3 has also demonstrated the field trial of a 4-ch 40Gb/s OFDM/N-OTDM transmission, over the 89.2-km JGN X test bed. We use WSSs both at the TX, and RX, for system reconfigurability; compared to conventional OFDM experiments with the same architecture, we achieve a large PAPR reduction, without affecting the spectral efficiency and energy consumption per bit [25-38].

7.1 Field trial through 89.2-km JGN-X test bed

Figure 39 shows the field trial for a 40 Gb/s OFDM/N-OTDM transmission through the 89.2-km JGN-X test bed. Since the available WSS has only 4 input ports, we could transmit only 4 adjacent independent subcarriers (ch 1,2,3,4), with the maximum spectral efficiency; a large number of subcarriers can be generated using an AWG. The laser source is a 10-GHz mode locked laser diode (MLLD), with 1.5 ps pulse width (full width at half maximum) and 193.245 THz center frequency. The pulse train is differentially binary phase shift keying (DBPSK) modulated by 10 Gb/s pseudo random bit sequence (PRBS) with a pattern length of 2^{31}-1. The 10 Gb/s DBPSK modulated signal is split into 4, and different delays are applied using optical delay lines (ODL), for synchronization and pattern decorrelation. The signals are fed to the input ports of the 4×1 WSS (Finisar 4000S) at the TX, to generate a 40 Gb/s hybrid OFDM/N-OTDM signal that is transmitted through the 89.2 km JGN-X test bed; dispersion is compensated by a dispersion compensation module (DCM). At the RX, a 1×1 WSS (Finisar 1000S) is used, and we suitably change the filtering function to separately receive the four subcarriers. Finally, the output signal is time-gated by a LN-IM. The eye diagrams of the four received subcarriers are shown in Fig. 40(a), and we observe a clear eye opening. Figure 40(b) shows the bit error rate (BER) measured as a function of the received power, which is largely below the FEC-limit (2×10^{-3}).

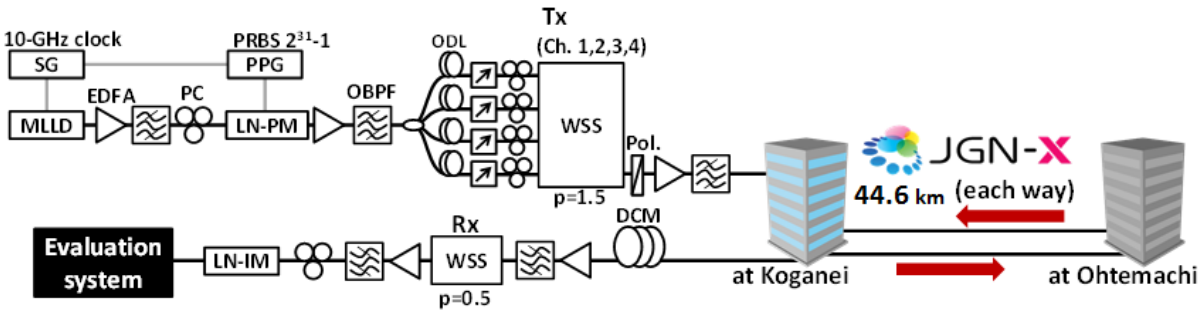

Figure 39 Experimental setup for DQPSK modulated OFDM transmission using 4 Fr-FT subcarriers.

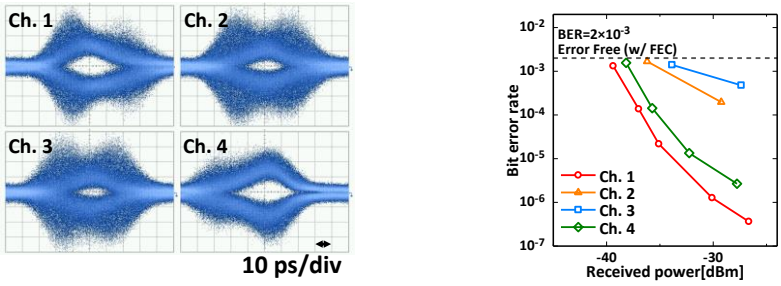

(a) (b)

Figure 40 (a) Eye diagram of the received FrFT subcarriers after time gating (b) BER performance of the 4 FrFT subcarriers.

The intermediate subchannels 2 and 3 present the worse performance, because they suffer for larger inter-carrier interference (ICI), due to the large time gating interval (~50 ps). System performances can be enhanced reducing the gating interval.

7.2 OFDM/N-OTDM: measured performances

To demonstrate the OFDM/N-OTDM capability, we have used the same experimental setup of Fig. 39, without the test bed. In this case, we have transmitted 6 (over 12) Fr-FT subcarriers (ch 1,2,3,6,7,8), to generated a 60 Gb/s hybrid OFDM/N-OTDM signal, whose spectrum is shown in Fig. 41(a). For the OFDM RX (Fig. 41(a)), we use a WSS at the TX, and Fig. 41(b) shows the eye diagrams of 3 received subcarriers, after time-gating. For the N-OTDM RX, we replace the WSS with a 25-km single mode fiber (instead of a DCF) with dispersion parameter D=435 ps/nm. Fig. 41(e) shows the eye diagrams of the N-OTDM signal; the width of the *sinc*-shaped pulse is $T\tan(p\pi/2)$=34.5 ps.

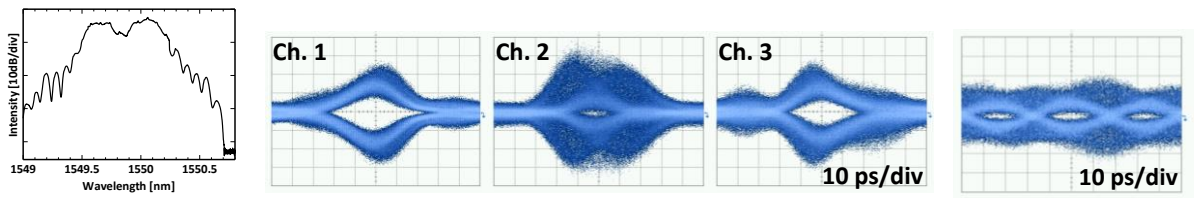

(a) (b) (c)

Figure 41. (a) 60 Gb/s hybrid OFDM/N-OTDM spectrum, Eye diagrams of (b) three OFDM subcarriers, (c) N-OTDM signal.

References for sections 6 and 7

[1]. A. J. Lowery, and L. B. Du, "All-optical OFDM transmitter design using AWGRs and low-bandwidth modulators," Opt. Express 19(17), 15696-15704 (2011). Avalaible at: https://www.osapublishing.org/oe/abstract.cfm?uri=oe-19-17-15696

[2]. L. B. Du, J. Schroeder, J. Carpenter, B. Eggleton, and A. J. Lowery, "Flexible all-optical OFDM using WSSs," in Proc. Optical Fiber Communication Conference (2013), paper PDP5B.9.

[3]. J. Hoxha, J. Morosi, S. Shimizu, P. Martelli, P. Boffi, N, Wada, and G. Cincotti, "Spectrally-efficient all-optical OFDM by WSS and AWG," Opt. Express 23(9), 10986-10996 (2015). Avaliable at: https://www.osapublishing.org/oe/abstract.cfm?uri=oe-23-9-10986

[4]. Z. Wang, K. S. Kravtsov, Y. K. Huang, and P. R. Prucnal, "Optical FFT/IFFT circuit realization using arrayed waveguide gratings and the applications in all-optical OFDM system," Opt. Express,

19(5), 4501–4512 (2011). Avaliable at: https://www.osapublishing.org/oe/abstract.cfm?uri=oe-19-5-4501.

[5]. A. J. Lowery, and L. B. Du, "All-optical OFDM transmitter design using AWGRs and low-bandwidth modulators," Opt. Express 19(17), 15696-15704 (2011). Avalaible at: https://www.osapublishing.org/oe/abstract.cfm?uri=oe-19-17-15696

[6]. S. Shimizu, G. Cincotti, and N. Wada," Demonstration and performance investigation of all-optical OFDM systems based on arrayed waveguide gratings," Opt. Express 20(26), 525-534 (2012). Available at: https://www.osapublishing.org/oe/abstract.cfm?uri=oe-20-26-B525

[7]. S. Shimizu, G. Cincotti, N. Wada, "Chromatic dispersion monitoring and adaptive compensation in an 8 x 12.5 G/s all-optical OFDM system," European Conference on Optical Communication (ECOC), London, UK 2013.

[8]. J. Hoxha, G. Cincotti, N. Diamantopoulos, P. Zakynthinos, I. Tomkos, "All-optical implementation of OFDM/NWDM Tx/Rx," invited paper International Conference on Optical Transparent Networks (ICTON) Cartagena, Spain 2013.

[9]. J. Hoxha, G. Cincotti, "Performance limits of all-optical OFDM systems," invited paper International Conference on Optical Transparent Networks (ICTON) Cartagena, Spain 2013.

[10]. J. Hoxha, G. Cincotti, M. Nazarathy, P. Zakynthinos, I. Tomkos, "Software defined transceivers for high-speed flexible optical networks," Future Network & MobileSummit 2013, Lisbon, Portugal 2013.

[11]. J. Hoxha, G. Cincotti, "System performance of coherent all-optical OFDM in long-haul transmission," 15o Convegno Nazionale sulle Tecniche Fotoniche nelle Telecomunicazioni (FOTONICA), Milan, Italy 2013.

[12]. P. Zakynthinos, G. Cincotti, M. Nazarathy, R. Kaiser, Polina Bayvel, R. I. Killey, M. Angelou, S. B. Ezra, M. Irion, A. Tolmachev, B. Gomez Saavedra, J. Hoxha, V. Grundlehner N. Psaila, G. Vollrath, R. Magri, G. Papastergiou, I. Tomkos, "Advanced hybrid integrated transceivers to realize flexible terabit networking," IEEE Photonics Society Newsletter, 28, 1, 12-19 February (2014).

[13]. J. Hoxha, G. Zarra, G. Cincotti, "A flexible and spectrally efficient OFDM system for unbundling the local loop in optical access networks," 19th European Conference on Network and Optical Communications (NOC), Milan, Italy, June 2014.

[14]. P. Martelli, P. Parolari, L. Marazzi, L. Blundetto, M. Martinelli G. Cincotti, "High-capacity access networks based on hybrid all-optical OFDM PON," 19th European Conference on Network and Optical Communications (NOC) Milan, Italy, June 2014.

[15]. J. Hoxha, G. Zarra, G. Cincotti, "OFDM-based solutions for unbundling the local loop in optical access networks," 16 Convegno Nazionale sulle Tecniche Fotoniche nelle Telecomunicazioni (FOTONICA), Naples, Italy 2014.

[16]. J. Morosi, P. Boffi, P. Martelli, P. Parolari, G. Cincotti, S. Shimizu, N. Wada, "Hybrid OFDM experimentation by all-optical FFT implementation," Convegno Nazionale delle Tecnologie Fotoniche FOTONICA, Torino 2015.

[17]. J. Morosi, J. Hoxha, P. Boffi, P. Martelli, G. Cincotti, S. Shimizu, N. Wada, "QPSK-based all-optical OFDM with direct and coherent detection," Convegno Nazionale delle Tecnologie Fotoniche FOTONICA, Torino 2015.

[18]. J. Morosi, G. Cincotti, P. Martelli, P. Parolari, J. Hoxha, N. Wada, S. Shimizu, P. Boffi, "25-Gb/s per user coherent all-optical OFDM for Tb/s-capable long-reach PONs," OSA Journal of Communications and Networks, accepted.

[19]. J. Hoxha, S. Shimizu, N. Wada, G. Cincotti, "FBG- and AWG-based AO-OFDM demultiplexing," Photonics in Switching (PS), Florence, Italy 2015.

[20]. P. Boffi, P. Martelli, P. Parolari, L. Blundetto, J. Morosi, G. Cincotti, "Demonstration and performance investigation of hybrid OFDM systems for optical access network applications," IEEE Photon. J.,vol. 7, no. 1, article # 7900309, 2015.

[21]. J. Morosi, P. Boffi, P. Martelli, P. Parolari, G. Cincotti, S. Shimizu, N. Wada, "Hybrid OFDM experimentation based on arrayed waveguide grating for all-optical FFT implementation in a PON architecture," IET Electronics Letters, 51, 22, 1802-1804 (2015).

[22]. P. Boffi, P. Martelli, P. Parolari, L. Marazzi, L. Blundetto, M. Martinelli, G. Cincotti, "Hybrid all-optical OFDM for access PON," 16 Convegno Nazionale sulle Tecniche Fotoniche nelle Telecomunicazioni (FOTONICA), Naples, Italy 2014.

[23]. G. Cincotti, S. Shimizu, T. Murakawa, T. Kodama, K. Hattori, M. Okuno, S. Mino, A. Himeno, T. Nagashima, M. Hasegawa, N. Wada, H. Uenohara, T. Konishi, "OFDM to OTDM conversion by optical fractional Fourier transform," invited paper Photonics in Switching San Diego California 2014.

[24]. G. Cincotti, S. Shimizu, T. Murakawa, T. Kodama, K. Hattori, M. Okuno, S. Mino, A. Himeno, T. Nagashima, M. Hasegawa, N. Wada, H. Uenohara, T. Konishi, "Flexible power-efficient Nyquist-OTDM transmitter, using a WSS and time-lens effect," Optical Fiber Communication Conference (OFC), Los Angeles, California 2015.

[25]. G. Cincotti, "All-optical and fully-passive Nyquist OTDM transmission and OFDM demultiplexing,"Keynote speach 9th international workshop on Optical Signal Processing and Optical Switching (IWOO)", Osaka 2014.

[26]. G. Cincotti, S. Shimizu, T. Murakawa, T. Kodama, K. Hattori, M. Okuno, S. Mino, A. Himeno, T. Nagashima, M. Hasegawa, N. Wada, H. Uenohara, T. Konishi, "OFDM to OTDM conversion by fractional Fourier transform" invited paper International Topical Meeting on Microwave Photonics/9th Asia Pacific Microwave Photonics (MWP/APMP 2014), Sapporo, Japan 2014.

[27]. T. Konishi, T. Murakawa, T. Nagashima, S. Shimizu, M. Hasegawa, K. Hattori, M. Okuno, S. Mino, A. Himeno, N. Wada, H. Uenohara, G. Cincotti, "Fractional-OFDM transmission for time/frequency multiplexing in elastic networks," invited paper Asia Communications and Photonics (ACP), Honk Kong 2015.

[28]. G. Cincotti, 'Time-frequency photonics signal processing,' Optoelectronics and Communications Conference/International Conference on Photonics in Switching2016 (OECC/PS2016), invited paper Toki Messe, Niigata, Japan.

[29]. T. Konishi, G. Cincotti, T. Kodama, T. Murakawa, T. Nagashima, M. Hasegawa, S. Shimizu, N. Wada, "Study on transmission technology using optical fractional discrete Fourier transform device for optical OFDM," Japanese Domestic Workshop of IEICE Photonic Network March 2014.

[30]. T. Murakawa, T. Nagashima, M. Hasegawa, S. Shimizu, G. Cincotti, K. Hattori, M. Okuno, S. Mino, A. Himeno, N. Wada, H. Uenohara, T. Konishi, "Emulation technique for AWG-based optical fractional OFDM device development by WSS," 9th International workshop on Optical Signal Processing and Optical Switching (IWOO), Osaka 2014.

[31]. T. Murakawa, G. Cincotti, S. Shimizu, T. Nagashima, M. Hasegawa, K. Hattori, M. Okuno, S. Mino, A. Himeno, N. Wada, H. Uenohara, T. Konishi, "Fractional OFDM transmitter and receiver for time/frequency multiplexing in gridless, elastic networks," Optical Fiber Communication Conference (OFC), Los Angeles, California 2015.

[32]. G. Cincotti, T. Konishi. "Time frequency optical multiplexing, or in between?" FIAT-LUX conference, Rome 2015.

[33]. T. Nagashima, G. Cincotti, T. Murakawa, S. Shimizu, M. Hasegawa, K. Hattori, M. Okuno, S. Mino, A. Himeno, N. Wada, H. Uenohara, T. Konishi, "PAPR management of all-optical OFDM signal using fractional Fourier transform for fibre nonlinearity mitigation," 41th European Conference on Optical Communication (ECOC), Valencia, Spain 2015.

[34]. T. Nagashima, G. Cincotti, T. Murakawa, S. Shimizu, M. Hasegawa, K. Hattori, M. Okuno, S. Mino, A. Himeno, N. Wada, H. Uenohara, T. Konishi, "Insertion of cyclic prefix for all-optical fractional OFDM," Photonics in Switching (PS), Florence, Italy 2015.

[35]. T. Nagashima, G. Cincotti,T. Murakawa, S. Shimizu, M. Hasegawa, K. Hattori, M. Okuno, S. Mino, A. Himeno, N. Wada, H. Uenohara, T. Konishi "Cost effective fractional OFDM receiver using arrayed waveguide grating," Optoelectronics and Communications Conference/International Conference on Photonics in Switching2016 (OECC/PS2016), Toki Messe, Niigata, Japan.

[36]. M. Hiraoka, T. Nagashima, B. Karanov, G. Cincotti, S. Shimizu, T. Murakawa, M. Hasegawa, K. Hattori, M.Okuno, S. Mino, A. Himeno, N. Wada, H. Uenohara, T. Konishi "Optical serial-to-parallel conversion based on fractional OFDM scheme," Optoelectronics and Communications Conference/International Conference on Photonics in Switching2016 (OECC/PS2016), Toki Messe, Niigata, Japan.

[37]. G. Cincotti, "Enhanced functionalities of AWGs," IEEE/OSA Journal of Lightwave Technology 33, 5, 998-1006 (2015).

[38]. T. Konishi, T. Murakawa, T. Nagashima, M. Hasegawa, S. Shimizu, K. Hattori, M. Okuno, S. Mino, A. Himeno, H. Uenohara, N. Wada, G. Cincotti, "Flexible OFDM-based access systems with intrinsic function of chromatic dispersion compensation," invited paper for the Topical Issue of Optical Fiber Technology on Next Generation Optical Access Networks.26, 94-99 (2015).